

Hopf bifurcation and time periodic orbits in reaction–diffusion systems with pde2path

Hannes Uecker

Institut für Mathematik, Universität Oldenburg, D26111 Oldenburg, hannes.uecker@uni-oldenburg.de

May 11, 2019

Abstract

We describe how to treat Hopf bifurcations and continuation of periodic orbits for systems of PDEs in 1, 2 and 3 spatial dimensions in the **Matlab** continuation and bifurcation package **pde2path**. The setup is explained by three examples, a complex Ginzburg–Landau equation, a reaction diffusion system on a disk, and an extended Brusselator system with interaction of Turing and Turing–Hopf bifurcations. The package (library and demos) can be downloaded at www.staff.uni-oldenburg.de/hannes.uecker/pde2path.

Contents

1	Introduction	2
2	Hopf bifurcation and periodic orbit continuation in pde2path	3
2.1	Branch and Hopf point detection	3
2.2	Branch switching	5
2.3	The continuation of Hopf branches	6
2.3.1	General setting	6
2.3.2	Arclength parametrization	6
2.3.3	Natural parametrization	9
2.4	Further remarks	9
3	Download, installation, help, and data structures	9
4	Three examples	11
4.1	OOPDE, and general remarks	11
4.2	A complex Ginzburg–Landau equation: Demo cGL	12
4.3	Rotating patterns on a disk: Demo rot	16
4.4	An extended Brusselator: Demo bru	18
5	Summary and discussion	21
A	Assembly using TOM	22
B	hopflib library overview	23
C	Some implementation details	25

1 Introduction

The package `pde2path` [UWR14, DRUW14] was developed as a continuation/bifurcation package for stationary problems of the form

$$G(u, \lambda) := -\nabla \cdot (c \otimes \nabla u) + au - b \otimes \nabla u - f = 0, \quad (1)$$

with various types of boundary conditions (BC). Here $u = u(x) \in \mathbb{R}^N$, $x \in \Omega \subset \mathbb{R}^2$, some bounded domain, $\lambda \in \mathbb{R}^p$ is a parameter (vector), and $c \in \mathbb{R}^{N \times N \times 2 \times 2}$, $b \in \mathbb{R}^{N \times N \times 2}$, $a \in \mathbb{R}^{N \times N}$ and $f \in \mathbb{R}^N$ can depend on $x, u, \nabla u$, and parameters. It has been applied to various research problems, e.g., patterns in 2D reaction diffusion systems [UW14, Kue15b, Kue15a, SDE⁺15, Wet16] including so called snaking of localized patterns, some problems in fluid dynamics and nonlinear optics [ZHKR15, DU16] and, with the add-on package `p2poc`, in optimal control [Uec16a].

We have revised `pde2path` to also work efficiently for $\Omega \subset \mathbb{R}^d$ with $d = 1, 3$. This extension is based on replacing `Matlab`'s `pdetoolbox` by the free FEM implementation `OOPDE` [Prü16]. This can also be used in 2D, which makes `pde2path` independent of the `pdetoolbox`, and with unified user interfaces in 1D, 2D and 3D. Moreover, we are adding new features, and the main purpose of this note is to explain new `pde2path`-functions, collected in a library `hopflib`, to treat Hopf bifurcations and the continuation of time-periodic orbits for systems of the form

$$\partial_t u = -G(u, \lambda), \quad u = u(x, t), \quad x \in \Omega \subset \mathbb{R}^d, \quad d = 1, 2, 3, \quad t \in \mathbb{R} \quad (d + 1 \text{ dimensional problem}). \quad (2)$$

Of course, adding the time dimension makes computations more expensive, such that here we focus on 1D and 2D, and only give one 3D example to illustrate that all user interfaces are essentially dimension independent, and thus this manual also serves as an introduction to the new `pde2path` setup. However, details on 3D computations (with focus on the stationary case) will appear elsewhere.

To explain the setup and usage of `hopflib` we use three example problems, with the source code included in the package download at [Uec16b] as demo directories. The first is a cubic-quintic complex Ginzburg-Landau (cGL) equation, which we consider over 1D, 2D, and 3D cuboids with homogeneous Neumann and Dirichlet BC, such that we can explicitly calculate all Hopf bifurcation points (HBP) from the trivial branch. For periodic boundary conditions we also have the Hopf branches explicitly, which altogether makes the cGL equation a nice toy problem to validate and benchmark the `hopflib` routines. Our second and third examples are somewhat more involved. In §4.3 we consider a reaction diffusion system from [GKS00] on a circular domain and with somewhat non-standard Robin BC, which lead to rotating waves. Our third example is a Brusselator system from [YDZE02] which shows interesting interactions between Turing branches and Turing-Hopf branches, see §4.4.

The goal of `pde2path` continues to be a general and easy to use (and modify and extend) toolbox to investigate solutions of PDEs of the (rather large) class of PDEs given by (2). With `hopflib` we provide some basic functionality to study Hopf bifurcations for such PDEs over 1D, 2D, and 3D domains, where at least the 1D and 2D case are sufficiently fast to use `pde2path` as a quick (i.e., interactive) tool for studying interesting problems. The user interfaces reuse the standard `pde2path` setup (with the addition of `OOPDE`), and no new user functions are necessary. Due to higher computational costs in 2+1D, in 3D, or even 3+1D, compared to the 2D case from [UWR14], in this tutorial we work with quite coarse meshes, but give a number of comments on numerical accuracy and on how to efficiently generate and work with finer meshes.

In §2 we review some basics of Hopf bifurcation and its numerical treatment in `pde2path`, in §3 we review the `pde2path` installation, basic data structures and the help system, in §4 we present the examples, in §5 we give a brief summary, and in the Appendices we collect information on the pertinent new `pde2path` fields, functions and switches, and some implementation details.

Acknowledgement. Many thanks to Francesca Mazzia for providing the BVP package TOM [MT04], which was essential help for setting up `hopf1ib`, and to Uwe Prüfert for providing OOPDE.

2 Hopf bifurcation and periodic orbit continuation in `pde2path`

For general reviews on (numerical) continuation and bifurcation we recommend [Gov00, Kuz04, Doe07, Sey10], and [Mei00], which has a focus on reaction–diffusion systems. Our following description of the algorithms is based on the spatial FEM discretization of (2), which, with a slight abuse of notation, we write as

$$M\dot{u}(t) = -G(u(t), \lambda), \quad (3)$$

where $M \in \mathbb{R}^{n_u \times n_u}$ is the mass matrix, $n_u = Nn_p$ is the number of unknowns (degrees of freedom DoF), where n_p is the number of mesh-points, and, for each t ,

$$u = (u_{1,1}, \dots, u_{1,n_p}, u_{2,1}, \dots, u_{N,1}, \dots, u_{N,n_p}) \in \mathbb{R}^{n_u},$$

and similarly $G : \mathbb{R}^{n_u} \times \mathbb{R}^p \rightarrow \mathbb{R}^{n_u}$. As in [UWR14, DRUW14] we assume that the problem is described by the `Matlab` struct `p`, with its various subfields such as `p.nc`, `p.sw` and `p.fuha` for the numerical controls, switches, and function handles. We use the general name λ for the parameter vector, and the *active* continuation parameter, again see [DRUW14] for details. When in the following we discuss eigenvalues μ and eigenvectors ϕ of the linearization

$$M\dot{v} = -\partial_u G(u, \lambda)v \quad (4)$$

of (3) around some (stationary) solution of (3), or simply eigenvalues of $\partial_u G = \partial_u G(u, \lambda)$, we always mean the generalized eigenvalue problem

$$\mu M\phi = \partial_u G\phi. \quad (5)$$

Thus eigenvalues of $\partial_u G$ with *negative* real parts give dynamical *instability* of u .

2.1 Branch and Hopf point detection

Hopf bifurcation is the bifurcation of a branch of time periodic orbits from a branch $\lambda \mapsto u(\cdot, \lambda)$ of stationary solutions of (2), or numerically (3). Roughly speaking, this generically occurs if at some $\lambda = \lambda_H$ a pair of simple complex conjugate eigenvalues $\mu_j(\lambda) = \bar{\mu}_{j+1}(\lambda)$ of $G_u = \partial_u G(u, \lambda)$ crosses the imaginary axis with nonzero imaginary part and nonzero speed, i.e.,

$$\mu_j(\lambda_H) = \bar{\mu}_j(\lambda_H) = i\omega \neq 0, \quad \text{and } \mu'_j(\lambda_H) \neq 0. \quad (6)$$

Thus, the first issue is to define a suitable test function ψ_H to detect (6). Additionally, we also want to detect real eigenvalues crossing the imaginary axis, i.e.,

$$\mu_j(\lambda_{BP}) = 0, \quad \text{and } \mu'_j(\lambda_{BP}) \neq 0. \quad (7)$$

A fast and simple method for (7) is to monitor sign changes of the product

$$\psi(\lambda) = \prod_{i=1, \dots, n_u} \mu_i(\lambda) = \det(G_u) \quad (8)$$

of all eigenvalues, which even for large n_u can be done quickly via the *LU* factorization of G_u , respectively the extended matrix in arclength continuation, see [UWR14, §2.1]. This so far has

been the standard setting in `pde2path`, flagged by `p.sw.bifcheck=1`, but the drawback of (8) is that the sign of ψ only changes if an odd number of real eigenvalues crosses 0.

Unfortunately, there is no general method for (6) which can be used for large n_u . For small systems, one option would be

$$\psi_H(\lambda) = \prod_i (\mu_i(\lambda) + \mu_{i+1}(\lambda)), \quad (9)$$

where we assume the eigenvalues to be sorted by their real parts. However, this, unlike (8) requires the actual computation of all eigenvalues, which is not feasible for large n_u . Other options are, e.g., diadic products, [Kuz04, Chapter 10], which again are not feasible for large n_u .

If, on the other hand, we assume that (2) is a parabolic problem, then we may try to just compute n_{eig} eigenvalues of G_u of smallest modulus, which, for moderate n_{eig} can be done efficiently, and to count the number of eigenvalues in the left complex half plane, and from this detect both (6) and (7). The main issue then is to choose n_{eig} , which unfortunately is highly problem dependent, and for a given problem may need to be chosen large again. Nevertheless, this has already been an option in `pde2path`, flagged by `p.sw.bifcheck=2`.

Another method [GS96] uses complex analysis, namely the winding number $W(g(i\omega), 0, \infty)$ of $g(z) = c^T(G_u - zM)^{-1}b$, which is the Schur complement of the bordered systems $\begin{pmatrix} G_u - zM & b \\ c^T & 0 \end{pmatrix}$ with (some choices of) $b, c \in \mathbb{R}^{n_u}$. We have

$$g(z) = \frac{N(z)}{\det(G_u - zM)}, \quad \text{where } W(g(i\omega), 0, \infty) = \pi(Z_l - Z_r + P_r - P_l)/2, \quad (10)$$

where $Z_{l,r}, P_{l,r}$ are the zeros and poles of $g(z)$ in the left and right complex half planes, respectively, and where N is a polynomial in z which depends on b, c . Since $\det(G_u - zM)$ does not depend on b, c , using some clever evaluation [GS96] of (10) for some choices of b, c one can count the poles of g , i.e. the generalized eigenvalues of G_u in the left half plane.

Here we basically refine the `p.sw.bifcheck=2` (counting small eigenvalues) setup using some ideas from the winding number setup from [GS96]. Instead of just counting eigenvalues near the “shift” 0, we also provide (one or more) shifts $\omega_{1,2,\dots}$ and compute (few) eigenvalues near $i\omega_l$ to see if some of these cross the imaginary axis. To estimate suitable shifts ω_l , given a current solution (u, λ) we compute

$$[0, \omega_{\max}] \ni \omega \mapsto g(u, \lambda, i\omega; b) := b^T(G_u - i\omega)^{-1}b, \quad (11)$$

for one or several suitably chosen $b \in \mathbb{R}^{n_u}$. This generically will be large for $i\omega$ near some complex eigenvalue $\mu = \mu_r + i\mu_i$, and thus we may consider this $i\omega$ as a *candidate* for a Hopf eigenvalue during the next continuation steps. To accurately compute g from (11) we refine the ω discretization using ideas from [GS96] (and actually compute the winding number), and then compute about 3-5 eigenvalues near the shifts $0, \omega_1, \dots$, during each continuation step. In general we can always reset the shifts after a number of continuation steps by evaluating (11) again, and instead of (11) the user can also set $\omega_{1,2,\dots}$ by hand.

Of course, the idea is mainly heuristic, and may miss some HBP, and can and typically will detect false bifurcation points, see Fig. 1, which illustrates that the algorithm can fail in various ways. Some of these failures can be detected and/or corrected, but of course these corrections (computing more eigenvalues, resetting ω_1) are not for free.¹ In practice, however, we found the

¹A third typical kind of failure is that during a continuation step a number m of eigenvalues crosses the imaginary axis close to $i\omega_1$, and simultaneously m already unstable eigenvalues leave the pertinent circle to the left due to a decreasing real part. The only remedy for this is to decrease the step-length ds . Clearly, a too large ds can miss bifurcations even if we could compute *all* eigenvalues, for instance if along the true branch eigenvalues cross back and forth.

algorithm to work remarkably well in a number of examples, with a rather small numbers of eigenvalues computed near 0 and $i\omega_1$, e.g., `p.nc.neig=[4 4]`, and in general to be more robust than the theoretically more sound usage of (10).² See Table 1 for an overview of the bifurcation detection setup, and §4 for examples.

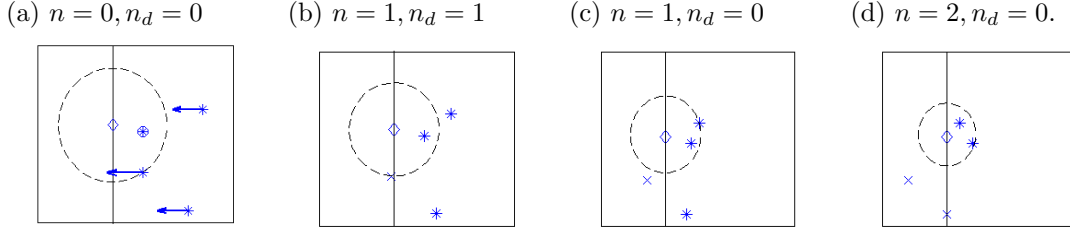


Figure 1: Sketch of the idea, and typical failures, of detecting Hopf points by counting eigenvalues with negative real parts near some shift $i\omega_1$, marked by \diamond . Here, for illustration we use `neig=2`, i.e., use the 2 eigenvalues closest to $i\omega_1$ for bifurcation detection, and show 4 eigenvalues near $i\omega_1$, stable ones with $*$ and unstable ones with \times . n is the total number of negative eigenvalues, and n_d the number of detected ones. From (a) to (d) we assume that some parameter λ varies, and the shown eigenvalues depend continuously on λ ; for better illustration we assume that the eigenvalue circled in (a) stays fixed. The dashed circle has radius $|\mu(\lambda) - i\omega_1|$ with μ the second closest eigenvalue to $i\omega_1$. From (a) to (b) we correctly detect a HBP. From (b) to (c) we incorrectly find a HBP, as the only unstable eigenvalue wanders out of the pertinent circle. From (c) to (d) we miss a HBP, as the guess $i\omega_1$ is too far off. The failure (b) to (c) can be detected in the localization by requiring that at the end the real part of the eigenvalue closest to the imaginary axis is sufficiently small. The failure from (c) to (d) can be resolved by either (i) computing more eigenvalues close to $i\omega_1$, or (ii) by updating $i\omega_1$ using (11).

Table 1: Setting of `p.sw.bifcheck`

bifcheck	method, comments
0	Just continuation, no detection of bifurcation at all.
1	Use (8); fast, reliable, but only detects an odd number of eigenvalues crossing the imaginary axis, hence no Hopf.
2	Compute <code>p.nc.neig(j)</code> eigenvalues nearest to the shifts <code>p.nc.eigref(j)</code> , and for each $j = 0, 1, \dots, j_{\max}$ count the number of those with negative real-part. General, can detect (6) and (7), but can falsely detect bifurcation points.

After detection of a BP or a HBP, or of several of these along a branch between s_0 and $s_0 + ds$, it remains to locate the BP or HBP. Again, there are various methods to do this, using, e.g., suitably extended systems [Gov00]. However, so far we restrict to a simple bisection, which works well and sufficiently fast in our examples.

A located BP or HBP is saved to disk as `p.file.dir/bpt[bpcount]` or `p.file.dir/hpt[hpcount]`, respectively, where `bpcount` and `hpcount` are counters, and BPs will moreover be indicated by `p.sol.ptype=1`, while HBPs have by `p.sol.ptype=3`. As before, BPs are indicated by a \circ in bifurcation diagrams, while HBPs have \diamond .

2.2 Branch switching

Branch switching at a BP works as usual by computing an initial guess from the normal form of the stationary bifurcation, see [UWR14, §2.1]. Similarly, to switch to a Hopf branch of time periodic

²However, if additionally to bifurcations one is interested in the stability of (stationary) solutions, then the values in `p.nc.neig` should not be chosen too small; otherwise the situation in Fig. 1(c,d) may easily occur, i.e., undetected negative eigenvalues.

solutions we compute an initial guess from an approximation of the normal form

$$\dot{w} = \mu(\lambda)w + c_1(\lambda)|w|^2w, \quad (12)$$

of the bifurcation equation on the center manifold associated to $(\lambda, \mu) = (\lambda_H, \omega_H)$. Thus we use

$$\mu(\lambda) = \mu_r(\lambda) + i\mu_i(\lambda) = \mu'_r(\lambda_H)(\lambda - \lambda_H) + i(\omega_H + \mathcal{O}(\lambda - \lambda_H)) + \mathcal{O}((\lambda - \lambda_H)^2) \quad (13)$$

and with $w = re^{i\omega_H t}$ replace (12) by

$$0 = r(\mu'_r(\lambda_H)(\lambda - \lambda_H) + c_1(\lambda_H)|r|^2). \quad (14)$$

Following [Kuz04], $c_1 = c_1(\lambda_H) \in \mathbb{R}$ is related to the first Lyapunov coefficient l_1 by $c_1(\lambda_H) = \omega_H l_1$, and we use the formulas from [Kuz04, p531-536] for the numerical computation of l_1 . Setting $\lambda = s\varepsilon^2$ with $s = \pm 1$ we then have a nontrivial solution

$$r = \varepsilon\alpha, \quad \alpha = \sqrt{-s\mu'(\lambda_H)/c_1(\lambda_H)} \quad (15)$$

of (14) for $s = -\text{sign}(\mu'(\lambda_H)/c_1)$, and thus take

$$\lambda = \lambda_H + s\varepsilon^2, \quad u(t) = u_0 + 2\varepsilon\alpha \text{Re}(e^{i\omega t}\Psi), \quad (16)$$

as an initial guess for a periodic solution of (3) with period near $2\pi/\omega$. The approximation (16) of the bifurcating solution in the center eigenspace, also called linear predictor, is usually accurate enough, and is the standard setting in the routine `p=hoswibra(dir,pt,ds,para,aux)`, where `dir` and `pt` determine the Hopf point previously saved to file, `ds` corresponds to the step length ε in (16), where `para=3` or `para=4` distinguishes between natural (by λ) vs arclength parametrization of the bifurcating branch, and where `aux` as usual may be used to pass additional arguments, see App. B. The coefficients $s = \pm 1$ and α in (16) are computed, and ε is then chosen in such a way that the initial step length is `ds` in the norm (20) below.

2.3 The continuation of Hopf branches

2.3.1 General setting

The continuation of the Hopf branch is, as usual, a predictor–corrector method, and for the corrector we offer, essentially, two different methods, namely natural (`p.sw.param=3`) and arclength (`p.sw.param=4`) continuation. For both, we reuse the standard `pde2path` settings for assembling G in (2) and Jacobians, such that the user has to provide no new functions. To assemble the discrete systems for (3), and for `p.sw.param=3` to also solve them, we use the BVP solver package TOM [MT04] in an adaption called `mtom` which incorporates M on the left hand side of (3). In any case, first we rescale $t = Tt$ in (3) to obtain

$$M\dot{u} = -TG(u, \lambda), \quad u(\cdot, 0) = u(\cdot, 1), \quad (17)$$

with unknown period T , but with initial guess $T = 2\pi/\omega$ at bifurcation.

2.3.2 Arclength parametrization

We start with the arclength setting, which is more general and more robust, although our natural continuation has other advantages such as error control and adaptive mesh refinement for the time discretization, see below. We add the phase condition

$$\phi := \int_0^1 \langle u(t), M\dot{u}_0(t) \rangle dt \stackrel{!}{=} 0, \quad (18)$$

where $\dot{u}_0(t)$ is from the previous continuation step, and the steplength condition

$$\psi := \xi_H \sum_{j=1}^m \langle u(t_j) - u_0(t_j), u'_0(t_j) \rangle + (1 - \xi_H) [w_T(T - T_0)T'_0 + (1 - w_T)(\lambda - \lambda_0)\lambda'_0] - ds \stackrel{!}{=} 0, \quad (19)$$

where again T_0, λ_0 are from the previous step, ds is the step-length, $' = \frac{d}{ds}$ denotes differentiation with respect to arclength, ξ_H and w_T denote weights for the u and T components of the unknown solution, and $t_0 = 0 < t_1 < \dots < t_m = 1$ is the temporal discretization. Thus, the steplength is ds in the weighted norm

$$\|(u, T, \lambda)\|_\xi = \sqrt{\xi_H \sum_{j=1}^m \|u(t_j)\|_2^2 + (1 - \xi_H) [w_T T^2 + (1 - w_T) \lambda^2]}. \quad (20)$$

Even if ξ_H is similar to the (average) mesh-width in t , then the term $\xi_H \sum_j \|u(t_j)\|_2$ is only a crude approximation of the “natural length” $\int_0^1 \|u(t)\|_2 dt$. However, the choice of the norm is somewhat arbitrary, and we found (20) most convenient. Typically we choose $w_T = 1/2$ such that T and λ have the same weight in the arclength (19). A possible choice for ξ_H to weight the number mn_u of components of u is

$$\xi_H = \frac{1}{mn_u}. \quad (21)$$

However, in practice we choose $\xi_H = \frac{10}{mn_u}$, or even larger (by another factor 10), since at the Hopf bifurcation the branches are “vertical” ($\|u - u_0\| = \mathcal{O}(\sqrt{|\lambda - \lambda_0|})$, cf. (16)), and ξ_H tunes the search direction in the extended Newton loop (26) between “horizontal” (large ξ_H) and “vertical” (small ξ_H). See [UWR14, §2.1] for the analogous role of ξ for stationary problems.

The integral in (18) is discretized as a simple Riemann sum, such that the derivative of ϕ wrt u is, with $\tilde{u}_0(t) = M\dot{u}_0(t)$,

$$\partial_u \phi = (h_1 \tilde{u}(t_1)_1, \dots, h_1 \tilde{u}(t_1)_{n_u}, h_2 \tilde{u}(t_2)_1, \dots, h_2 \tilde{u}(t_2)_{n_u}, \dots, h_{l-1} \tilde{u}(t_{m-1})_{n_u}, 0, \dots, 0), \quad (22)$$

n_u zeros at the end, where $h_l = t_{l+1} - t_l$ is the mesh-size in the time discretization. Similarly, denoting the tangent along the branch as

$$\tau = (\tau_u, \tau_T, \tau_\lambda), \quad \tau_u \in \mathbb{R}^{1 \times mn_u} \text{ (row vector as in (22))}, \quad \tau_T, \tau_\lambda \in \mathbb{R}, \quad (23)$$

we can rewrite ψ in (19) as

$$\psi = \xi_H \tau_u (u - u_0) + (1 - \xi_H) (w_T \tau_T (T - T_0) + (1 - w_T) \tau_\lambda (\lambda - \lambda_0)) - ds. \quad (24)$$

Setting $U = (u, T, \lambda)$, and writing (17) as $\mathcal{G}(u, T, \lambda) = 0$, in each continuation step we thus need to solve

$$H(U) := \begin{pmatrix} \mathcal{G}(U) \\ \phi(u) \\ \psi(U) \end{pmatrix} \stackrel{!}{=} \begin{pmatrix} 0 \\ 0 \\ 0 \end{pmatrix} \in \mathbb{R}^{mn_u+2}, \quad (25)$$

for which we use Newton’s method, i.e.,

$$U^{j+1} = U^j - A(U^j)^{-1} H(U^j), \quad A = \begin{pmatrix} \partial_u \mathcal{G} & \partial_T \mathcal{G} & \partial_\lambda \mathcal{G} \\ \partial_u \phi & 0 & 0 \\ \xi_H \tau_u & (1 - \xi_H) w_T \tau_T & (1 - \xi_H) (1 - w_T) \tau_\lambda \end{pmatrix}. \quad (26)$$

After convergence of U^j to U , i.e., $\|H(U)\| \leq \text{"tolerance"}$ in some suitable norm, the next tangent τ_1 with preserved orientation $\langle \tau_0, \tau_1 \rangle > 0$ can be calculated as usual from

$$\mathcal{A}(U)\tau_1 = (0, 0, 1)^T. \quad (27)$$

It remains to actually assemble \mathcal{G} in (17) and the Jacobian $\partial_u \mathcal{G}$. For this we use (modifications of) routines from TOM, which assumes the unknowns in the form

$$y = (y(t_1), y(t_2), \dots, y(t_l)). \quad (28)$$

Thus, we accordingly reshape (the column) vector $(u_{i,j}(t_l))_{i,j,l}$ into a matrix $y \in \mathbb{R}^{n_u \times m}$. As TOM requires separated boundary conditions we also need to suitably pad y to implement the periodic boundary conditions in t . Afterwards, however, we can simply invoke TOM to compute the terms in (3), including derivatives such as $\partial_u \mathcal{G}(U)$ needed in (26). See Appendix A for details.

Remark 2.1. $\mathcal{A} \in \mathbb{R}^{(mn_u+2) \times (mn_u+2)}$ in (26), (27) consists of $A = \mathcal{G}_u \in \mathbb{R}^{mn_u \times mn_u}$, which is large but sparse, and borders of widths 2, i.e., symbolically,

$$\mathcal{A} = \begin{pmatrix} A & B \\ C & D \end{pmatrix}, \text{ with large and sparse } A, \text{ with } C^T, B \in \mathbb{R}^{mn_u \times 2}, \text{ and } D \in \mathbb{R}^{2 \times 2}.$$

There are various methods to solve bordered systems of the form

$$\mathcal{A}x = b, \quad b = \begin{pmatrix} f \\ g \end{pmatrix}, \quad (29)$$

see, e.g., [Gov00]. Here we use the very simple scheme

$$V = A^{-1}B, x_1 = A^{-1}f, \tilde{D} = D - CV, y_1 = g - Cx_1, y_2 = \tilde{D}^{-1}y_1, x_2 = x_1 - Vy_2, x = \begin{pmatrix} x_1 \\ x_2 \end{pmatrix}. \quad (30)$$

The big advantage of such bordered schemes is that solving systems such as $Ax_1 = f$ (where we either prefactor A for repeated solves, or use a preconditioned iterative method) is usually much cheaper due to the sparsity structure of A than solving $\mathcal{A}x = (f, g)$ (either by factoring \mathcal{A} , or by an iterative method with some preconditioning of \mathcal{A}). The scheme (30) is implemented in the `hopflib` function `mbe1`. It may suffer from some instabilities, but often these can be corrected by a simple iteration: If $\|r\|$ with $r = \mathcal{A}x - b$ is too large, then we solve $\mathcal{A}\hat{x} = r$ (again by (30), which is cheap) and update $x = x - \hat{x}$, until $\|r\| \leq \text{"tolerance"}$. Very rarely we obtain poor solutions of (29) for $b = (0, 0, 1)^T$ from (27), which moreover cannot be improved by iteration, and in this case we use $x = \mathcal{A} \setminus b$ to solve (29). Altogether we found the scheme (30) to work well in our problems, with a typical speedup of up to 50 compared to the naive direct solution $x = \mathcal{A} \setminus b$ of (29). Again, see [Gov00] for alternative schemes and detailed discussion.

For the solutions of $AV = B$ and $Ax_1 = f$ in (30) we give the option to use a preconditioned iterative solver from `ilupack` [Bol11]. For this, the user may set `p.hopf.ilss=1` before calling `p=cont(p)`, see the examples in §4. The (initial) computation of the ilu-preconditioner, the calls to the iterative solvers, and the update of the preconditioner when needed, then happen in `mbe1`. The number of continuation steps along a (nontrivial) before a new preconditioner is needed can be quite large, and often the iterative solvers give a significant speedup. However, this of course is strongly problem dependent. Thus, the iterative option in `mbe1` should rather be seen as somewhat experimental, and the default settings as a template for building problem adapted solvers; see [Bol11] for further details.]

2.3.3 Natural parametrization

By keeping λ fixed during correction we cannot pass around folds, but on the other hand can take advantage of further useful features of TOM. Since, as already said, TOM requires separated boundary conditions, we use a standard trick and introduce, in the notation (28), auxiliary variables $\tilde{y} = (\tilde{y}_1, \tilde{y}_2, \dots, \tilde{y}_m)$ and additional (dummy) ODEs $\dot{\tilde{y}}_l = 0$. Then setting the boundary conditions

$$y_1 - \tilde{y}_1 = 0, \quad y_m - \tilde{y}_m = 0 \quad (31)$$

corresponds to periodic boundary conditions for y . Moreover, we add the auxiliary equation $\dot{T} = 0$, and set up the phase condition

$$\phi = \langle u(0), M\dot{u}_0(0) \rangle \stackrel{!}{=} 0. \quad (32)$$

as an additional boundary condition. Thus, the complete system to be solved is

$$\begin{pmatrix} M\dot{y} \\ \dot{\tilde{y}} \\ \dot{T} \end{pmatrix} = \begin{pmatrix} -G(y) \\ 0 \\ 0 \end{pmatrix}, \quad (33)$$

together with (31) and (32). We may then pass an initial guess (from a predictor) at a new λ to TOM, and let TOM solve for (y, \tilde{y}) and T . The main benefit is that this comes with error control and adaptive mesh refinement for the temporal discretization. See §4 for examples.

2.4 Further remarks

So far we do not provide options for directly tracking (via Floquet multipliers) the stability of the bifurcating Hopf solutions, or for detecting bifurcations *from* the Hopf branches, e.g., period doubling (flip) or Neimark–Sacker bifurcations [DGK03, Kuz04]. However, we can assess the stability of the Hopf-solutions by using the time-integration routines from `pde2path`.

3 Download, installation, help, and data structures

The package and demos, and older `pde2path` manuals and further information can be found at and downloaded from [Uec16b]. The file `pde2path.tar.gz` (or `pde2path.zip`) unpacks to the root-directory `pde2path`, which contains the directory tree shown in Fig. 2(a), where `demos` contains the stationary `pde2path` demos, `hopfdemos` contains demos described in this work, `html` contains the Help system, `libs` contain the `pde2path` libraries, `ocdemos` contains the optimal control demos described in [Uec15], and `OOPDElightNA` is a “light” version of OOPDE, with No Abstract classes for compatibility with older `Matlab` versions.

To get started, in `Matlab`, change into the `pde2path` directory and run `setpde2path`, which also makes available the help system. Calling `p2phelp` yields the Main help menu shown in Fig. 2(b). The first two topics are short thematic overviews of the data structures and main functions in `pde2path`, while clicking `p2plib`, `...`, `tom` yields complete alphabetic function overviews of these `pde2path` libraries, with a very short description of each function, which can then be clicked for documentation.³ Similarly, clicking on `demos` opens the demo overview in (d), with brief descriptions of and pertinent links to the demo directories.

As already said, see [UWR14] and in particular [DRUW14] for the basic organization of the `pde2path`-struct `p` describing a given problem, which however for convenience we briefly recall in

³Of course, help on any `pde2path` function `foo` is also given by typing `help foo` or `doc foo`, but in practice we find the alphabetic library overviews such as in Fig. 2(c) most convenient.

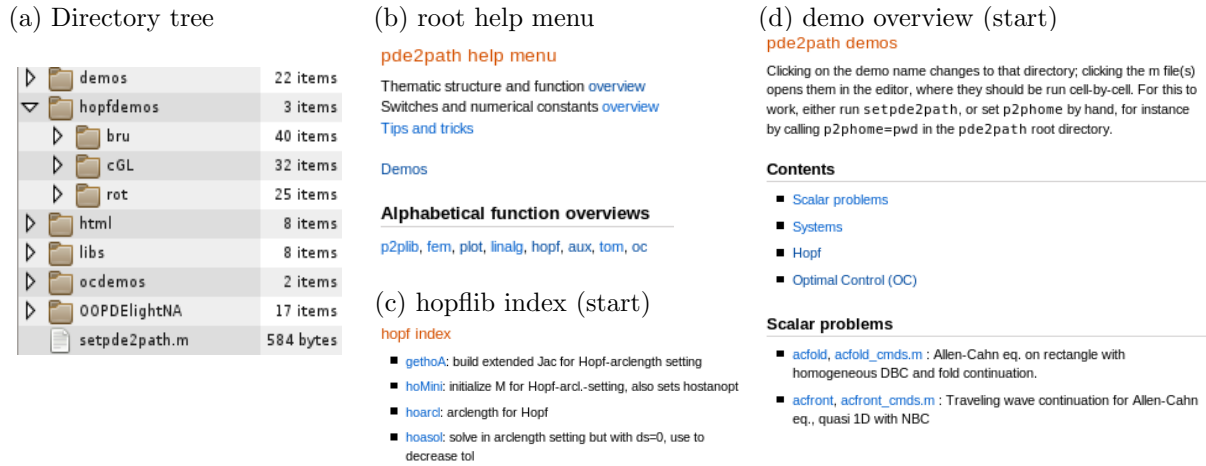


Figure 2: Directory tree, Root help menu, and starting parts of `hopflib` index and demo overview.

Table 2, where the last two lines contain new fields described in this guide. Both are supplementary in the sense that they are not generated or used for purely stationary `pde2path` demos; `p.pdeo` is initialized at startup if the user chooses the OOPDE setup described in §4.1, while `p.hopf` is initialized by `hoswibra`, i.e., by a switching to a Hopf branch.

Table 2: Fields in structure `p`; see [DRUW14] for a review of the contents of (and standard settings in) these fields, except for `p.pdeo`, `p.hopf`, described in §4.1 and §B, respectively. See also the html help or `stanparam.m` for further information.

field	purpose	field	purpose
fuha	f unction h andles, e.g., <code>fuha.G</code> , ...	nc	n umerical c ontrols, e.g., <code>nc.tol</code> , ...
sw	s witches such as <code>sw.bifcheck</code> , ...	sol	values/fields calculated at runtime
eqn	tensors c, a, b for fast FEM setup	mesh	the geometry data and mesh
plot	switches and controls for plotting	file	switches etc for file output
time	timing information	pm	pmcont switches
fsol	switches for the <code>fsolve</code> interface	nu,np	# PDE unknowns, # meshpoints
u,tau	solution and tangent	branch	branch data
usrlam	vector of user set target values for the primary parameter, default <code>usrlam=[]</code> ;		
mat	problem matrices, in general data that is not saved to file		
pdeo	OOPDE data if OOPDE is used, see [Prü16] for documentation		
hopf	Hopf data, initialized in <code>hoswibra</code>		

To get started with the `hopfdemos`,

- change into one of the `hopfdemos` directories, and open `*cmds.m`; here `*` stands for `cGL`, `rot`, `bru` and the spatial dimension, where we recommend to start with `cGL1dcmds`;
- execute `*cmds.m` cell by cell, and compare to the descriptions given in §4.2–4.4.

To set up your own problem, copy the demo directory which seems closest to your problem to a new directory, then modify the functions and scripts in it. See also the various demos in `demos`, described in [UWR14, DRUW14], for further tips and tricks regarding domains, BC, and the general setup of the pertinent G from (2).

To use `ilupack`, which we found useful in a number of demos, mex its `Matlab` interface, put `ilupacks */mex` directory in the `Matlab` path, and before calling `cont` set `p.hopf.ilss=1`. See also `mbel.m` in directory `hopflib/` concerning the standard settings for `ilupack` used in `hopflib`. The settings concerning `droptol`, `maxit` etc. are often problem dependent, and thus should be modified by copying `mbel.m` to your problem directory and modifying it there.

4 Three examples

4.1 OOPDE, and general remarks

Before presenting the demos we briefly comment on the new OOPDE setting in `pde2path`. OOPDE (object oriented PDE) [Prü16] is a free FEM package in `Matlab`. Inter alia, it provides, in 1D, 2D and 3D, most of the functionality that the `pdetoolbox` provides in 2D, and with somewhat similar basic interfaces. Thus, we use it to transfer the functionality of `pde2path` to 1D and 3D, and to also make `pde2path` independent of the `pdetoolbox` in 2D. A major difference, however, is the object oriented (OO) setup of OOPDE, which has some advantages [Prü16], such as tighter control of data access by the user and natural reuse resp. overload of methods by inheritance.

Currently we hardly use the OO aspects of OOPDE, i.e., our basic setup is as follows: There are three templates for creating pde-objects, namely the subclasses `stanpdeo1D`, `stanpdeo2D`, `stanpdeo3D` of the OOPDE class `pde`. These only set up simple domains (interval, rectangle, cuboid, respectively), the grids (intervals, triangles, tetrahedra) and the finite elements (piecewise linear continuous). Thus, calling, e.g., `p.pdeo=stanpdeo1D(1x,2*1x/nx)`, we have `pdeo` as a pde object in `p`, i.e., the 1D domain $\Omega = (-l_x, l_x)$ with a mesh of width $2l_x/n_x$, and, by default, linear Lagrange elements associated to it. This is already enough to, e.g., call `[K,M,dummyF]=p.pdeo.fem.assema(p.pdeo.grid,1,1,0)` to assemble the (one component) mass matrix M and stiffness matrix K (corresponding to the Neumann Laplacian), and there are very useful tools to set up boundary conditions as well. After some postprocessing, (to, e.g., create the needed matrices for systems of PDEs), we save these system matrices in `p.mat.K`, `p.mat.M`; see `oosetfemops` in the examples below. After this, we can implement all functions necessary to describe the system in a standard `pde2path` way. This way we only use a small subset of the OOPDE capabilities, but on the other hand stay close to the original `pde2path` setup.

The basic setup of all three demos (`cGL`, `rot`, `bru`) is similar: each demo directory first of all contains some function files such as `*init.m` for setting up the geometry and the basic `pde2path` data, where `*` stands for the problem, i.e., `cGL`, `rot` or `bru`. Then there are files `sG.m` and `sGjac.m` for setting up the rhs of the equation and its Jacobian. Here, somewhat different from the setup in [UWR14], we omit special names for these functions, i.e., they are just files `sG.m`, `sGjac.m` in each problem directory. Of course, one can still give individual names such as, e.g., `cGLsG.m`, and then set `p.fuha.sG=@cGLsG`, as opposed to us just setting `p.fuha.sG=@sG` for each problem. Moreover, we decided to *not* introduce a new function handle for the nonlinearity f in (1), which is needed in the computation of the coefficient α in the normal form (16); instead, we assume that f is encoded as `nodalf.m` in the problem directory, and of course we then also call `nodalf` in `sG.m`.⁴

Next, there are the main script files, such as `cGL*dcmds.m` where `*` stands for the space dimension, and the above mentioned `oosetfemops` files for setting up the system matrices, except for the demo `rot` where we use the old `pdetoolbox` setup. Additionally, there are a few auxiliary functions, for instance small modifications of the basic plotting routine `hoplot.m` from `hopflib`, which we found convenient to have problem adjusted a posteriori plots, while during continuation we use the standard `hoplot`. Finally, there are some auxiliary scripts `auxcmds.m`, which contain commands, for instance for creating movies or doing spatial mesh-refinement, which here we do not discuss in detail, but which we find convenient to illustrate either some mathematical aspects of the models, or some further `pde2path` capabilities, and which we hope the user will find useful as well.

In the following, we mostly focus on explaining the output of the main script files (i.e., the

⁴This assumes the semilinear setting, flagged by `p.sw.sfem=1` (`pdetoolbox`) or `p.sw.sfem=-1` (OOPDE), i.e., $\partial_t u = c\Delta u + au + b \otimes \nabla u + f(u)$, where $c, a \in \mathbb{R}^{N \times N}$ and $b \in \mathbb{R}^{N \times N \times 2}$ are fixed tensors, f is the only nonlinearity in (1), and the BC are linear as well. The computation of α is not yet supported for a full quasilinear problem, and thus the user should provide a guess, see the description of `hoswibra.m` in §B. However, so far all our examples are semilinear.

relevant plots), and on relating them to some mathematical background of the equations. Thus, for comments on implementation details, in particular for setting up the equations and Jacobians in `sG.m` and `sGjac.m` we mostly refer to the source files, and to [UWR14, DRUW14] and [Uec16b]. However, for our first example we also give some comments in Appendix C.

The script files `*cmds` are in cell mode, and we recommend to also execute them cell-by-cell to see the effect of the individual commands. Also note that some commands, e.g., the continuation of Hopf-branches in 3+1D, may take several minutes, so for `cGL` and `bru` we recommend to start with the 1D problems, where the numerics only take a few seconds.

4.2 A complex Ginzburg–Landau equation: Demo `cGL`

We consider

$$\partial_t u = \Delta u + (r + i\nu)u - (c_3 + i\mu)|u|^2 u - c_5|u|^4 u, \quad u = u(t, x) \in \mathbb{C}, \quad (34)$$

with real parameters r, ν, c_3, μ, c_5 . Using real variables u_1, u_2 with $u = u_1 + iu_2$, (34) can be written as a real 2-component system of the form (2), i.e.,

$$\partial_t \begin{pmatrix} u_1 \\ u_2 \end{pmatrix} = \begin{pmatrix} \Delta + r & -\nu \\ \nu & \Delta + r \end{pmatrix} \begin{pmatrix} u_1 \\ u_2 \end{pmatrix} - (u_1^2 + u_2^2) \begin{pmatrix} c_3 u_1 - \mu u_2 \\ \mu u_1 + c_3 u_2 \end{pmatrix} - c_5 (u_1^2 + u_2^2)^2 \begin{pmatrix} u_1 \\ u_2 \end{pmatrix}. \quad (35)$$

W.l.o.g. we set

$$c_3 = -1, c_5 = 1, \nu = \mu = 1, \quad (36)$$

and use r as the main bifurcation parameter. Considering (35) on, e.g., a (generalized) rectangle

$$\Omega = (-l_1\pi, l_1\pi) \times \cdots \times (-l_d\pi, l_d\pi) \quad (37)$$

with homogeneous Dirichlet BC or Neumann BC, or with periodic BC, we can explicitly calculate all Hopf bifurcation points from the trivial branch $u = 0$, and, for periodic BC, the bifurcating time periodic branches. For this let

$$u(x, t) = ae^{i(\omega t - k \cdot x)}, \text{ with wave vector } k = (k_1, \dots, k_d), k_j \in \frac{1}{2l_j}\mathbb{Z}, \quad (38)$$

and temporal period $2\pi/\omega$, which yields

$$|a|^2 = |a(k, r)|^2 = -\frac{c_3}{2c_5} \pm \sqrt{\frac{c_3^2}{4c_5^2} + r - |k|^2}, \quad \omega = \omega(k, r) = \nu - \mu|a|^2, \quad |k|^2 = k_1^2 + \dots + k_d^2. \quad (39)$$

Note that ω and hence the period $T = 2\pi/\omega$ depend on $|a|$, that $u(t, x)$ on each branch is a single harmonic in x and t , and that the phase of a is free. Using (36) we obtain subcritical Hopf bifurcations of solutions (38) at

$$r = |k|^2, \text{ with folds at } r = |k|^2 - \frac{1}{4}. \quad (40)$$

Thus, (35) makes a nice toy problem to validate and benchmark `hopflib` routines, if we restrict to pBC. However, as these are somewhat unphysical, here we rather use Neumann and Dirichlet BC, for which we still have the formula $r = |k|^2$ for the HBPs, although we lose the explicit branches, except the spatially homogeneous branch for $k = 0$ with Neumann BC.

Remark 4.1. An immediate consequence of the BC is that the solutions (38) have nodal sets, i.e., fixed subsets of Ω on which $u(x, t) = 0$ for all t , or equivalently $(u_1, u_2) = (0, 0)$. For simplicity restricting to 1D and Dirichlet BC, the general solution can be written as

$$u(x, t) = \sum_{n \in \mathbb{N}} a_n(t) \sin(nx/l), \quad a_n \in \mathbb{C}. \quad (41)$$

Then $\sin(nx/l) = 0$ on $|x| = lm/n$, $0 \leq m \leq n$, and the bifurcation at, e.g., $r = n_0/2l$ is into the invariant subspace

$$u(x, t) = \sum_{n \in \{n_0, 3n_0, 5n_0, \dots\}} a_n(t) \sin(nx/l),$$

i.e., the nodal structure is determined at bifurcation. The same conclusions hold for any spatial dimension d , and Neumann boundary conditions, and therefore, the bifurcation for (35) on cuboids (37) with Neuman or Dirichlet BC is always to *standing* (i.e., oscillatory) patterns. In §4.3 we will consider a similar problem on a circle, where suitable boundary conditions lead to the bifurcation of rotating patterns.]

The cGL demo directory consists, as noted above, of some function files to set up and describe (35), and some script files to run the simulations. As functions we have

- **cGLinit.m**, which (depending on the spatial dimension) sets up the domain, mesh, boundary conditions, and sets **p.fuha.sG=@sG** and **p.fuha.sGjac=@sGjac**;
- **sG.m** and **sGjac**, which encode (35) (after rewriting it as a 2-component real system) and the associated Jacobian of G , where **sG.m** calls **nodalf.m** which defines the nonlinearity;
- **oosetfemops.m**, which uses OOPDEs **assema** and **assemb** to set the system matrices;
- the auxiliary function **plotana** which plots the analytic branches (39).

Then we have three script files, **cGL*dcmds.m**, where $*$ =1,2,3 stands for the spatial dimension. These three files are basically equal. They only differ in setting filenames and some plotting commands, but the basic procedure is always the same:

1. call **cGLinit**, then **cont** to find the Hopf-bifurcation points;
2. compute Hopf branches by calling **hoswibra** and **cont** again, then plotting.
3. assess the stability of a periodic solution $t \mapsto u(\cdot, t)$ on a Hopf branch by using **hotintxs** to time integrate (35) with initial condition $u(\cdot, 0)$.

As already said, here we do not repeat all details about, e.g., translating (35) into **sG.m**, but give some brief remarks in Appendix C.

Because of our choice of the domain the eigenvalues of G_u are well separated in this example. Thus for the HBP detection we can safely use **bifcheck=2** with **neig=10**, and we postpone the discussion of problems which require preparatory calls to **initeig** to first estimate possible values for ω_1 (which here would be known a-priori as $\omega_1 = 1$) to §4.4.

In 1D we use Neumann BC, and $n_x = 30$ spatial, and (without mesh-refinement) $m = 20$ temporal discretization points. Just for illustration, in **cGL1dcmds.m** we compute the first two branches using the **para=4** (arclength) setting from the start, while for the third branch we first do 5 steps with **para=3** (nat.param.), where **tomsol** refines the starting t -mesh of 20 points to 40 points.⁵ This produces the plots in Fig. 3, where the norm in (a) is

$$\|u\|_* := \|u\|_{L^2(\Omega \times (0, T), \mathbb{R}^N)} / \sqrt{T|\Omega|}, \quad (42)$$

which is our default for plotting of Hopf branches. Additionally we remark that during the continuation **hoplot** also plots the time-series $t \mapsto u_1(x_0, t), u_2(x_0, t)$ for some mesh point x_0 , selected

⁵See also **cGL/auxcmds.m** for examples how to switch back and forth between **para=4** and **para=3** with the aim of error control and mesh refinement in t . We do not yet provide simultaneous in space and time error estimators and mesh-refinement, i.e., both work independently.

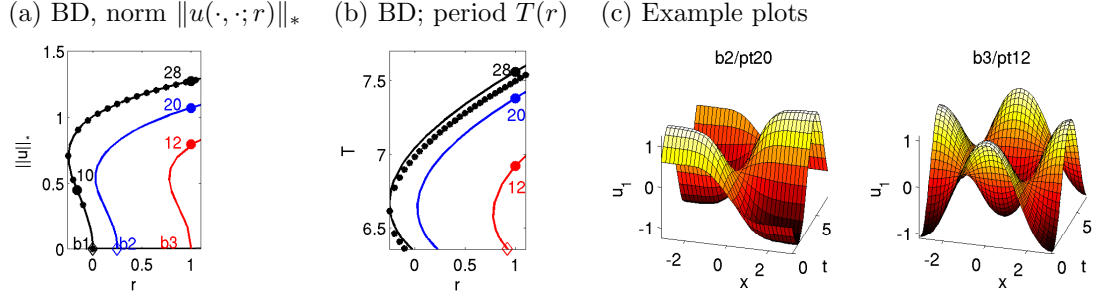


Figure 3: Numerical bifurcation diagrams and example plots for (35) on the domain $\Omega = (-\pi, \pi)$ with Neumann BC, 30 grid-points in x . Parameters $(\nu, \mu, c_3, c_5) = (1, 0.1, -1, 1)$, hence bifurcations at (restricting to the first three branches) $r = 0$ ($k = 0$, spatially homogeneous branch, black), $r = 1/4$ ($k = 1/2$, blue) and $r = 1$ ($k = 1$, red), see (40). The black dots in (a), (b) are the analytical solutions (39) with $k = 0$.

by the index `p.hopf.x0i`, which is set in `cGLinit` (see also Fig. 4). These simulations run in less than 10 seconds per branch on a i5 laptop computer, but the rather coarse meshes lead to some inaccuracies. For instance, the first three branch points, which analytically are at $r = 0, 1/4, 1$ are obtained at $r = 6 * 10^{-5}, 0.2503, 1.0033$, and (b) also shows some visible errors in the period T . However, these numerical errors quickly decay if we increase n_x and m , and runtimes stay moderate.

Switching to continuation in another parameter works just as for stationary problems by calling `p=swiparf`, but now followed by first setting `p.sw.para=3`, i.e., some initial steps in natural parametrization. See the end of `cGL1dcmds.m` for an example, and Fig. 4 for illustration.

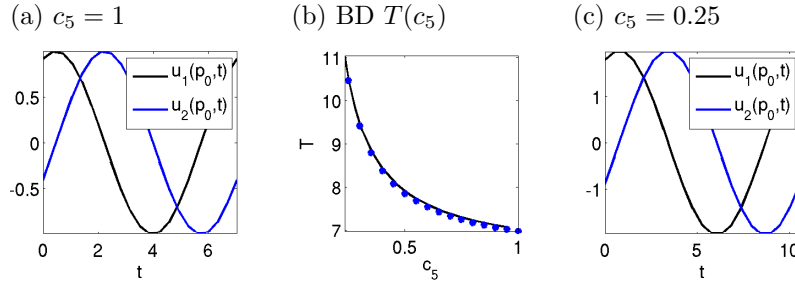


Figure 4: Continuing the solution b1/pt28 from Fig. 3(a,b) in c_5 . (a), (c) show $t \mapsto (u_1, u_2)(x_0, t)$ for some user selected x_0 (here arbitrary). In accordance with (39) the temporal dependence stays a single harmonic, and only the amplitude and period change. The blue dots in (b) are the analytical results (39).

Using Fig. 5 we briefly explain how to use the time integration routines of `pde2path` to assess the stability of Hopf-solutions. The idea is to start time integration from some point on the Hopf orbit, e.g. $u_0(\cdot) = u_H(\cdot, 0)$, and to monitor, inter-alia, $e(t) := \|u(t, \cdot) - u_0(\cdot)\|$, where by default $\|\cdot\| = \|\cdot\|_\infty$. Without approximation error for the computation of u_H (including the period T) and of $t \mapsto u(\cdot, t)$ we would have $e(nT) = 0$. In general, even if u_H is stable we cannot expect that, in particular due to errors in T which will accumulate with n , but nevertheless we usually can detect instability of u_H if at some t there is a qualitative change in the time-series of $e(t)$.⁶ In, e.g., Fig. 5(a), where we use the smaller amplitude periodic solution at $r = 0$ for the IC, this happens right from the start, but below we have examples where some instability of a periodic orbit only manifests after several periods. Panel (b) illustrates the stability of the larger amplitude periodic solution at $r = 0$, while in (c) with $r = 1$ we see the instability of the second Hopf branch ($r = 1$)

⁶ The time integration `hotintxs` takes inter alia the number `npp` of time steps per period T as argument. Time integration is of course much faster than the BVP solver used to compute the periodic orbits, and thus `npp` can be chosen significantly larger than the number `tl` of time-discretization points in BVP solver. Thus, choosing `npp=5*tl` or `npp=10*tl` appears a reasonable practice.

around $t = 11$, with subsequent convergence to the (stable) spatially homogeneous Hopf orbit.

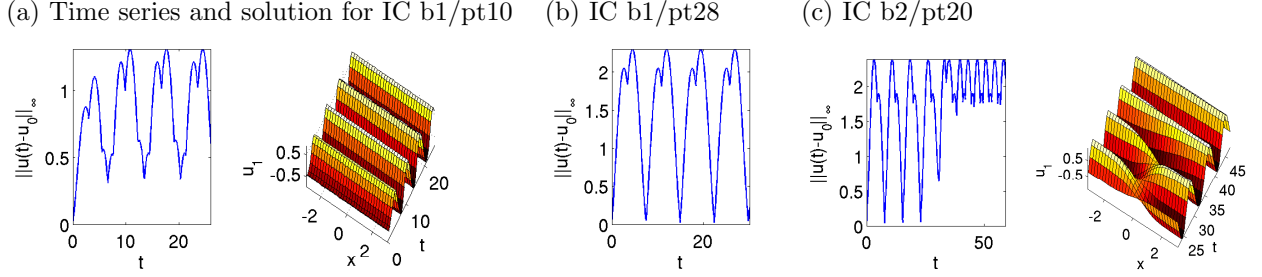


Figure 5: Stability experiments for (35) in 1D. (a) IC h1/pt10 (lower amplitude solution at $r \approx -0.16$), time series of $\|u(\cdot, t) - u_0\|_\infty$ and evolution, showing the convergence to the larger amplitude solution at the same r . (b) IC h1/pt29 from Fig. 3, where we plot $\|u(\cdot, t) - u_0\|_\infty$ for $t \in [0, 4T]$, which shows stability of the periodic orbit, and a good agreement for the temporal period under time integration. (c) instability of b2/pt26 from Fig. 3, and again convergence to the solution on the b1 branch. Note that the time-stepping is much finer than the appearance of the solution plots, but we only save the solution (and hence plot) every 100th step, cf. footnote 6.

Mainly to illustrate how to set up boundary conditions in OOPDE, in 2D we choose homogeneous Dirichlet BC for u_1, u_2 , see also the discussion of `oosetfemops.m` in Appendix C. Then the first two HBPs are at $r_1 = 5/4$ ($k = (1/2, 1)$), and $r_2 = 2$ ($k = (1, 1)$). Figure 6 shows some results obtained from `cGL2dcmds.m`, where again we use a rather coarse mesh of 26×13 points, hence $n_u = 676$ spatial unknowns, yielding the numerical values $r_1 = 1.262$ and $r_2 = 2.033$. With $m = 10$ temporal discretization points, the computation of each Hopf branch then takes less than a minute. Again, the numerical HBPs converge to the exact values when decreasing the mesh-size, but at the prize of longer computations for the Hopf branches. (c) illustrates the 2D analogue of Fig. 5(c), i.e., the instability of the second Hopf branch and stability of the first.

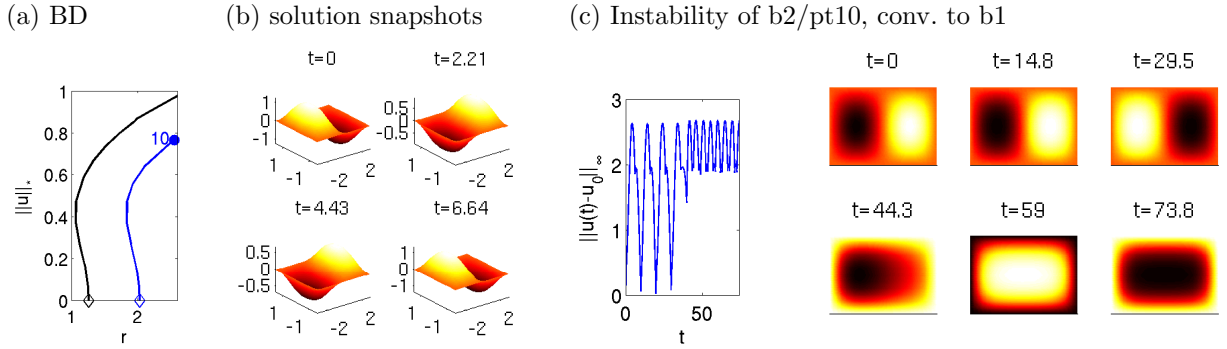


Figure 6: (a) Bifurcation diagrams of the first 2 Hopf branches for (35) in 2D. (b) Solution snapshot from b2/pt10, at $t = 0, \frac{3}{10}T, \frac{6}{10}T, \frac{9}{10}T$. (c) Time integration starting from (b) ($t = 0$), with convergence to the first Hopf branch.

To illustrate that exactly the same setup also works in 3D, in `cGL3dcmds.m` and Fig. 7 we consider (35) over $\Omega = (-\pi, \pi) \times (-\pi/2, \pi/2) \times (-\pi/4, \pi/4)$. Here we use a *very* coarse tetrahedral mesh of $n_p = 1386$ points, thus 2772 DoF in space. Analytically, the first 2 HBPs are $r_1 = 21/4$ ($k = (1/2, 1, 2)$) and $r_2 = 6$ ($k = (1, 1, 2)$), but with the coarse mesh we numerically obtain $r_0 = 5.7$ and $r_1 = 6.58$. Again, this can be greatly improved by, e.g., halving the spatial mesh width, but then the Hopf branches become very expensive. Using $m = 10$, the computation of the branches (with 10 continuation steps each) in Fig. 7 takes about 10 minutes on a I7 quadcore. For completeness we remark that solutions on b2 are unstable as expected, and time integration from an IC from b2 yields convergence to a periodic solution from b1.

The “slice plot” in Fig. 7(b), indicated by `p.plot.pstyle=1` should be used as a default setting, while the isolevels in (c) (via `p.plot.pstyle=2`) often require some fine tuning. Additionally we provide a “face plot” option `p.plot.pstyle=3`, which however is useless for Dirichlet BC. See the `hoplot.m` source for documentation of the plot options, and the ends of `cGLcmds2d.m` and `cGLcmds3d.m` for example plot calls, and on how to create movies, which can be found at [Uec16b].

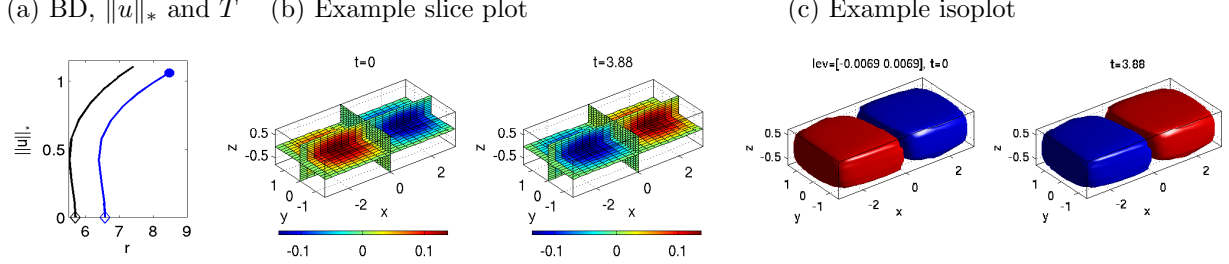


Figure 7: (a) Bifurcation diagram of first 2 Hopf branches for (35) in 3D. (b,c) Solution snapshots at $t = 0$ and $t = T/2$ for the blue dot in (a); slice-plot in (b), and isolevel plot in (c) with levels $0.525m_1 + 0.475m_2$ and $0.475m_1 + 0.525m_2$, where $m_1 = \min_{x,t} u_1(x, t)$ and $m_2 = \max_{x,t} u_1(x, t)$.

4.3 Rotating patterns on a disk: Demo rot

While the Hopf bifurcations presented in §4.2 have been to (standing) oscillatory patterns, cf. Remark 4.1, another interesting class is the Hopf bifurcation to rotating patterns. We follow [GKS00] and consider a real two component reaction diffusion system, somewhat similar to the cGL, but on the unit disk, and with Robin BC, namely

$$\partial_t u = d_1 \Delta u + (0.5 + r)u + v - (u^2 + v^2)u, \quad (43)$$

$$\partial_t v = d_2 \Delta v + rv - u - (u^2 + v^2)v, \quad (44)$$

$$\partial_n u + 10u = 0, \quad \partial_n v + 0.01v = 0,$$

where n is the outer normal, and where we take r as bifurcation parameter. Due to the BC (44), the eigenfunctions of the linearization around $(u, v) = (0, 0)$ are build from Fourier Bessel functions

$$\phi(\rho, \vartheta, t) = \text{Re}(e^{i(\omega t + m\vartheta)} J_m(q\rho)), \quad (45)$$

where (ρ, ϑ) are polar-coordinates, and with in general complex $q \in \mathbb{C} \setminus \mathbb{R}$, which has the consequence that the modes are growing in ρ , cf. the discussion in [GKS00].

The implementation follows the general remarks from §4.1, and we only point out that the circle is easily set up in `circgeo.m`, that the BC (44) are encoded in `nb.c.m`, and that here we only have one script file `rotcmds.m`. The homogeneous branch is stable up to $r \approx -0.21$, and Fig. 8(a) shows the first 6 bifurcating branches h_1, h_2, \dots, h_6 , from left to right, while (b) shows the spatial modes for h_1 - h_6 at bifurcation, with mode numbers $m = 0, 1, 2, 3, 2, 4$. We discretized (43), (44) with a mesh of 1272 points, hence $n_u = 2544$ DoF, and a very coarse temporal discretization of 10 points. Example plots of solutions on the Hopf branches are given in (e), with a temporal period near 2π for all branches.

The nontrivial solutions from Fig. 8(a),(e) are “rotations”, except for the spatial $m = 0$ mode h_1 . To discuss this, we return to (c),(d); in (c) we show the nodal lines for the components u, v at bifurcation of h_2 to h_5 (vector Ψ in (16)), and in (d) the linear predictors (16) for h_2 and h_3 (with $ds = 0.1$). The pertinent observation is that h_2 to h_6 (not shown) do not have nodal lines, i.e., $u(x)v(x) \neq 0$ except at $x = 0$.⁷ Thus, the branches h_2 to h_6 cannot consist of oscillatory

⁷The zero lines for h_3 are close together, but not equal; for h_1 we have $u(x, 0) < 0$ and $v(x, 0) > 0$ for all x .

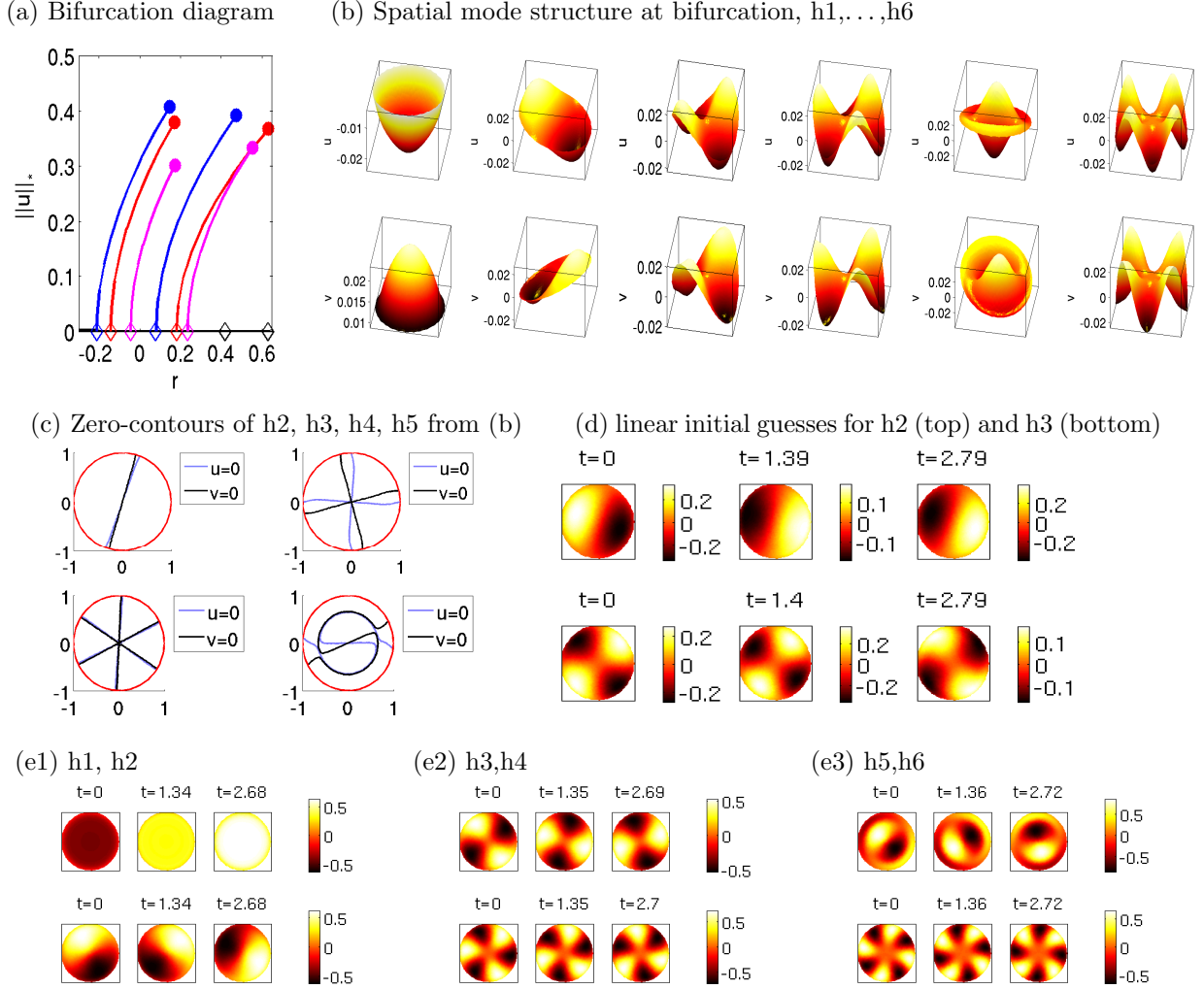


Figure 8: Basic bifurcation diagram (a) for (43), (44) with 10 continuation steps till the last points marked on the branches h1–h6 (left to right). (b)–(d): information on initial mode structure on the first five bifurcating branches; snapshots in (d) at $t = 0, 3T_j/14$ and $3T_j/7$, $T_j = 2\pi/\omega_j$. (e) Example plots at the marked points from (a). Snapshots of u at $t = 0, T_j/5$ and $2T_j/5$, with T_j the actual period.

patterns but must rotate. On the other hand, this rotation must involve higher order modes, and thus becomes more visible (and smoother, i.e., almost rigid) at larger amplitude. In particular, the component wise nodal lines for h2 are very close together, and therefore, in contrast to h3 a rotational motion is hardly visible in the linear predictor.

For further assessment of the numerical accuracy, in Table 3 we compare the numerical values for the Hopf points and the temporal wave number ω with the values from [GKS00], who compute r_4, r_5, r_6 , (and three more Hopf points) using semi analytical methods, and some numerics based on the `Matlab pdetoolbox` with fine meshes. Given our coarse mesh we find our results reasonably close, and again our values converge to the values from [GKS00] under mesh refinement.

Table 3: Comparison with [GKS00] (starred values).

r	-0.210	-0.141	-0.044	0.079	0.182	0.236
ω	0.957	0.967	0.965	0.961	0.953	0.957
r^*	NA	NA	NA	0.080	0.179	0.234
ω^*	NA	NA	NA	0.961	0.953	0.957

Finally, time-integration yields that all but the first Hopf branch $h1$ consist of unstable solutions, and that for $r > r_0 = -0.21$ solutions generically converge to a periodic orbit from $h1$. This is illustrated for an IC from $h3$ in Fig. 9. Nevertheless, see [GKS00] and [GS02, §4.7] for an interesting further discussion of the possible relevance of rotational modes as found above to spiral waves as for instance described in [HBK⁺96].

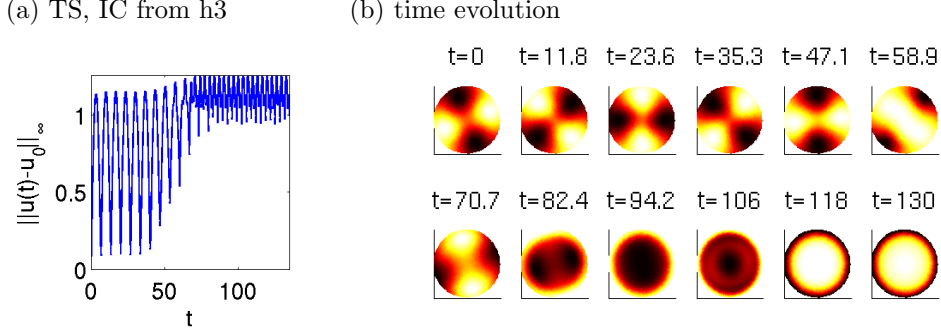


Figure 9: Time integration for (46); starting with IC from $h3/pt20$ the solution converges to the $h1$ branch.

4.4 An extended Brusselator: Demo bru

As an example where there is an interesting interplay between bifurcating stationary patterns and Hopf bifurcations, where there are typically many eigenvalues with small real parts, and where therefore detecting HBPs with `bifcheck=2` without first using `initeig` for setting a guess for a shift ω_1 is problematic, we consider an “extended Brusselator” problem from [YDZE02]. This is a three component reaction diffusion system of the form

$$\partial_t u = D_u \Delta u + f(u, v) - cu + dw, \quad \partial_t v = D_v \Delta v + g(u, v), \quad \partial_t w = D_w \Delta w + cu - dw, \quad (46)$$

where $f(u, v) = a - (1+b)u + u^2v$, $g(u, v) = bu - u^2v$, with kinetic parameters a, b, c, d and diffusion constants D_u, D_v, D_w . We consider (46) on rectangular domains in 1D and 2D, with homogeneous Neumann BC for all three components. The system has the trivial spatially homogeneous steady state

$$U_s = (u, v, w) := (a, b/a, ac/d),$$

and in suitable parameter regimes it shows co-dimension 2 points between Hopf, Turing–Hopf (aka wave), and (stationary) Turing bifurcations from U_s . We follow [YDZE02] and fix the parameters

$$(c, d, D_u, D_v, D_w) = (1, 1, 0.01, 0.1, 1). \quad (47)$$

Figure 10(a) then shows a characterization of the pertinent instabilities of U_s in the a, b plane. U_s is stable in region I, and can lose stability by (a, b) crossing the Turing line, which yields the bifurcation of stationary Turing patterns, or the wave (or Turing–Hopf) line, which yields oscillatory Turing patterns. Moreover, there is the “Hopf line” which corresponds to Hopf–bifurcation with spatial wave number $k = 0$.

In the following we fix $a = 0.95$ and take b as the primary bifurcation parameter. Figure 10(b) illustrates the different instabilities from (a), i.e.: as we increase b from 2.75, we first cross the Turing–Hopf line, with first instability at critical spatial wave number $k_{TH} \approx 0.7$, then the Hopf line, and finally the Turing line with critical wave number $k_T \approx 6.4$. To investigate the bifurcating solutions (and some secondary bifurcations) with `pde2path`, we need to choose a domain $\Omega = (-l_x/2, l_x/2)$ (1D), where due to the NBC l_x should be chosen as a (half integer) multiple of π/k_{TH} . For simplicity we take the minimal choice $l_x = 0.5\pi/k_{TH}$, which restricts the allowed

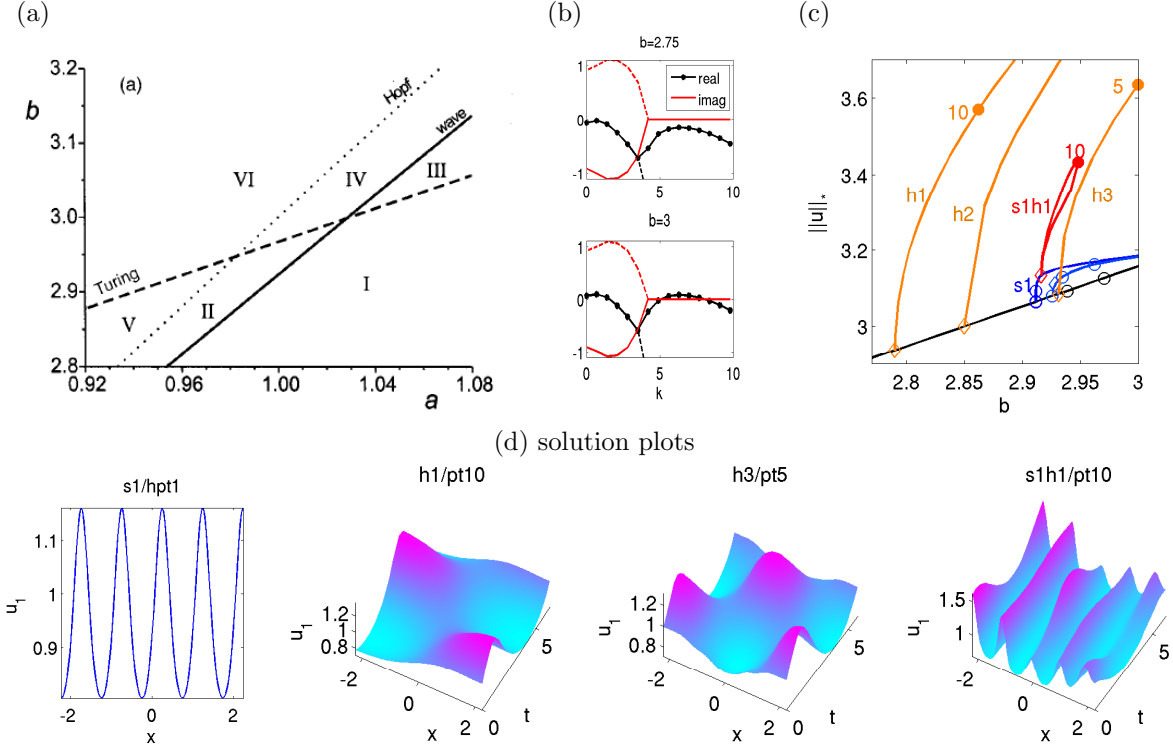


Figure 10: (a) Parameter plane with Hopf, Turing–Hopf (wave) and Turing instability lines for (46), reprinted with permission from [YDZE02], copyright 2002, AIP Publishing LLC. (b) Spectra for increasing b at $a = 0.95$. Contrary to the `pde2path` convention that due to $\partial_t u = -G(u)$ eigenvalues with *negative* real parts yield instabilities, here we directly plot the spectra of $-\partial_u G$, such that instability occurs for eigenvalues with positive real parts. The first instability (Turing–Hopf) occurs at $b \approx 2.794$, with $k_c \approx 0.7$. The admissible wave-numbers k on a domain $(-l_x, l_x)$ with $l_x = 0.5\pi/k_c$ are indicated by the dots. (c),(d): (partial) bifurcation diagram, and example plots on $\Omega = (-l_x, l_x)$.

wave numbers to multiples of k_{TH} , as indicated by the black dots in Figure 10(b). Looking at the sequence of spectral plots for increasing b , we may then *expect* first the TH branch h1 with $k = k_{\text{TH}}$, then a Hopf branch h2 with $k = 0$, then two Turing branches s1, s2 with $k = 6.3$ and $k = 7$, then a TH branch h3 with $k = 2k_{\text{TH}}$, and so on, and this is what we obtain from the numerics, as illustrated in (c) and (d).

Besides stationary secondary bifurcations we also get a rather large number of Hopf points on the Turing branches, and just as an example we plot the (Turing)Hopf branch s1h2 bifurcating from the second Hopf point on s2. The example plots in (d) illustrate that solutions on s1h1 look like a superposition of solutions on s1 and h1. Such solutions were already obtained in [YDZE02] from time integration, such that these solutions also have some stability properties, see also [YE03] for similar phenomena.⁸ However, by tracing out the various bifurcations this can be studied in a more systematic way. Moreover, in Fig. 11 we illustrate that s1h1/pt10 itself is not stable. Instead, after a transient near h3/pt5 (c) the solution converges to a solution from the primary Hopf branch h1 (d), which however itself also shows some short wave structure at this relatively large distance from bifurcation.

In 1D we may still use `bifcheck=2` without preparation to detect (and localize) the Hopf bifurcations, i.e., by computing a number (here 20) of eigenvalues closest to zero. In 2D this is unfeasible, because even over rather small domains we obtain many wave vectors $k = (k_1, k_2)$ with

⁸The branch bifurcating from the first Hopf point on s1 is a superposition of s1 and the uniform oscillations on h2, and thus graphically less interesting.

(a) “error” time series (b) initial evolution (c) transient near h3 (d) convergence to h1

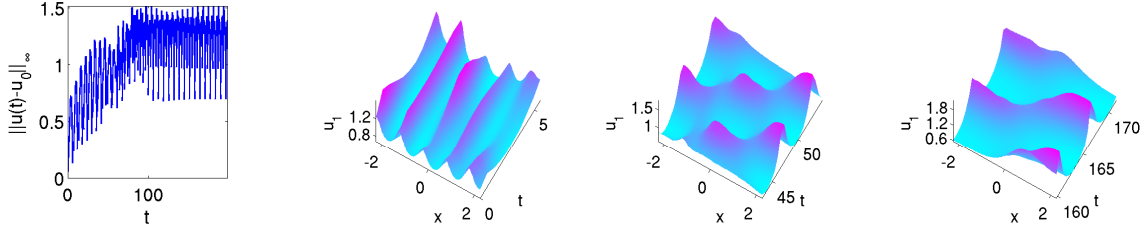


Figure 11: Instability of sh1h1/pt20. After a rather long transient near h3 the solution converges to an orbit on h1.

modulus $|k| \in (5, 8)$, which give leading eigenvalues $\mu_1(k)$ with small $\text{Re}\mu(k)$ and $\text{Im}\mu(k) = 0$. This is illustrated in Fig. 12, which shows that for $\Omega = (-0.5\pi/k_{\text{TH}}, 0.5\pi/k_{\text{TH}})^2$ even for $\text{neig}=200$ (which is quite slow already) we do not even see any Hopf eigenvalues, which become “visible” at, e.g., $\text{neig}=300$. Thus, here we first call `initwn` and `initeig` to generate a guess for the Hopf bifurcation (c); subsequently `bifcheck=2` with `neig=[10 10]` runs fast and reliable.

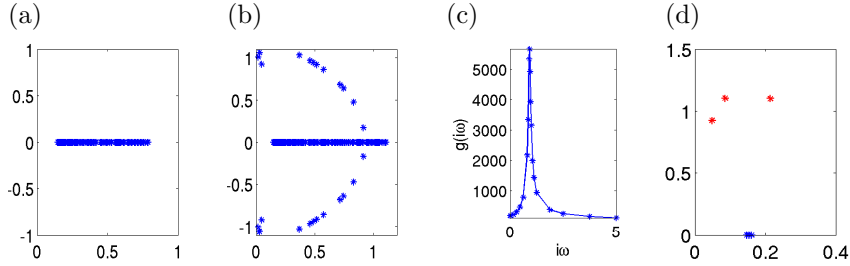


Figure 12: (a) Spectrum of the linearization of (46) around U_s at $b = 2.75$, remaining parameters from (47). Failure of `bifcheck=2` without preparation and too small $\text{neig}=200$. (b) $\text{neig}=300$. (c) calling `initeig` yields a guess $\omega = 0.9375$ for the ω value at Hopf bifurcation, and then using `bifcheck=2` with `neig=[3 3]` is reliable and fast: (d) shows the three eigenvalues closest to 0 in blue, and the three eigenvalues closest to $i\omega$ in red.

Finally, in Fig. 13 we give an example of just 4 of the many branches which can be obtained for (46) in 2D, even over quite small domains. We use $\Omega = (-l_x, l_x) \times (-l_y, l_y)$, $l_x = \pi/2$, $l_y = \pi/8$, which means that admissible wave vectors are $(k_1, k_2) = (n, 4m)$, $n, m \in \mathbb{N}_0$. Consequently, no spatial structure in y direction occurs in the primary Hopf branches (cf. Fig. 10b), i.e., the first three are just analogous to those in Fig. 10 and occur at $b = 2.818$ (with $k = (1, 0)$), $b = 2.859$ (with $k = (0, 0)$, i.e., spatially homogeneous, and hence b independent of the domain) and $b = 3.202$ (with $k = (2, 0)$); see (b2) for an example plot on the first Hopf branch. However, the first stationary bifurcation (at $b = 2.912$) is now to a spotted branch **2ds1**, see (b1), and stripe branches analogous to **1ds1** from Fig. 10 bifurcate at larger b . Moreover, while so far all branches were continued using `cont`, as usual for Turing branches in 2D (cf. [UWR14, §4]), the continuation of the branch **2ds1** is problematic with `cont` as this leads to undesired branch switching. Thus, in `br2dcmds.m` we use `pmcont` ([UWR14, §4.3]) to continue the **2ds1** branch.

Interestingly, after some stationary and Hopf bifurcations this branch becomes stable at $b = b_b \approx 2.785$, which illustrates that it is often worthwhile to follow unstable branches, as they may become stable, or stable branches may bifurcate from them. In particular, here for $b < b_b$ we have a bistability of the trivial branch and **2ds1**, and hence (over somewhat larger domains) phenomena such as heteroclinics between solutions on the trivial branch and on **2ds1**, and associated snaking branches of localized spots, see [UW14] and the references therein for related results in various models.

However, here we are interested in Hopf bifurcations from **2ds1**, and Fig. 13(b3,4) show example

plots on such a second secondary Hopf branch. Basically, these are again analogous to **s1h1** from Fig. 10, i.e., the solutions look like superpositions of the stationary pattern and solutions on the primary Hopf branch **h1**. (c) illustrates the dynamic instability of the spotted Hopf solutions; the spots stay visible for about 4 periods, and subsequently the solution converges to a periodic orbit from the primary Hopf branch, as in Fig. 11.

(a) BD, and u at 2nd HBP on blue branch (b) Hopf example plots (u) (c) Instability under time integration

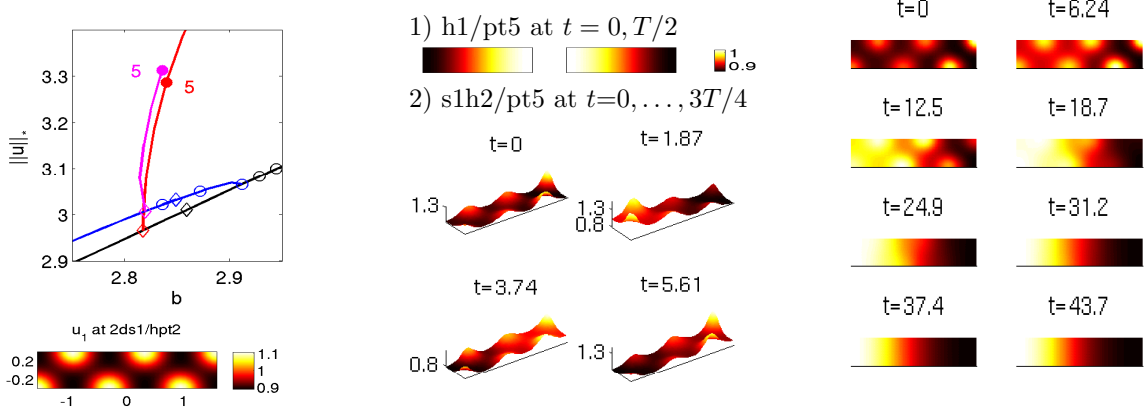


Figure 13: (a) Example bifurcations for (46) over a small 2D domain $\Omega = (-\pi/2, \pi/2) \times (-\pi/8, \pi/8)$, and example plots of u at 2nd Hopf point on the blue branch. (b) Example plots: solutions on primary Hopf branch (1), and on the secondary Hopf branch (2). (c) Time integration with $u(\cdot, 0)$ from 2ds1h2/pt5 (b2), snapshots at $0, T, 2T, \dots, 8T$.

Remark 4.2. As an example that besides the new functions from the **hopflib** we still have the full **pde2path** machinery available, in the script **auxcmds.m** we do some adaptive spatial mesh-refinement at the start of the (1D and 2D) Turing branches **1ds1** and **2ds1** and then continue.⁹ The further BPs and HBPs then obtained are very close at the BPs and HBPs on the coarser mesh, but the resolution of the bifurcating Hopf branches becomes considerably better, with a moderate increase of computation time, which in any case is faster than starting with a uniform spatial mesh yielding a comparable accuracy.]

5 Summary and discussion

With **hopflib** we provide the basic functionality to study Hopf bifurcations for the class (2) of PDEs over 1D, 2D and 3D domains, where at least the 1D and 2D case are sufficiently fast to use **pde2path** as a quick (i.e., interactive) tool for studying interesting problems. The user interfaces reuse the standard **pde2path** setup, and no new user functions are necessary. For the detection and localization of Hopf points we revised the **bifcheck=2** setting to detect eigenvalues crossing the imaginary axis near guesses $i\omega_j$, where the ω_j can either be set by the user (if such a priori information is available), or can be estimated via **initeig**, which is based on computing the function g from (11). An initial guess for a bifurcating periodic orbit is then obtained from the normal form

⁹In the OOPDE setting used here, mesh-adaption so far is implemented in 1D and 2D. Moreover, it works somewhat differently and is slightly less general than in the **pdetoolbox** setting, as follows: its local error estimator is the same as in the **pdetoolbox**, and needs a function $[c, a, f] = \text{eeG}(p, u)$ (“error estimate G ”) in the current directory, which returns the diffusion tensor c , the linear part a (usually $a=0$), and the nodal nonlinearity f . For f we can typically use the same **nodalf** which is also used in the normal form computation **hogetnf** or in setting up **sG**. See **eeG.m** in the **bru** demo directory. Note that there is no joint mesh adaption in t and x yet, and no mesh adaption in x on Hopf orbits.

(12), and the computation of the periodic orbits is based on modifications of the routines from TOM. The continuation of periodic orbits can be done in “natural” parametrization (`p.sw.param=3`), with the option of error control for the time discretization, or arclength continuation (`p.sw.param=4`), which appears somewhat faster and more robust, in particular in case of poor initial guesses. We explained the usage of the software using three example problems, where we believe that the second (demo `rot`) and the third (demo `bru`) are close to interesting research problems.

We do not yet provide functionality for tracking Floquet multipliers of periodic orbits, and thus do not yet consider bifurcations *from* Hopf branches. Basic stability checks can however be done with the time integration routines from `pde2path`.

Our OOPDE setup, with the goal of taking `pde2path` to 1D and 3D, does not yet provide the same flexibility concerning boundary conditions and fully nonlinear equations as the standard `pde2path` setup based on the Matlab `pdetoolbox`, see, e.g., `gnbc.m` and `gnbcs.m` in `pde2path`, or the examples in [UWR14, DRUW14]. Expert users, however, can find the relevant information for this in [Prü16]. Also, our usage of `ilupack` [Bol11] for the iterative solution with ILU preconditioning of linear systems is still rather basic. However, we plan to provide suitable interfaces to efficiently use `ilupack`, and to set up BC and quasilinear equations within OOPDE for the next update of `pde2path`, which will be concerned with a variety of (stationary) problems in 1D and 3D. Of course, this will also take compatibility with `hopflib` into account.

A Assembly using TOM

Here we collect, in mathematical notation, some details of the data structures used to call TOM to assemble (and for `p.sw.param=3` also solve) (3). For TOM, the (column vector)

$$u = (u_{1,1}(t=0), u_{1,2}(0), \dots, u_{1,n_p}(0), u_{2,1}(0), \dots, u_{2,n_p}(0), \dots, u_{N,n_p}(t=1))^T, \quad (48)$$

of unknowns, where $u_{i,j}(t_l)$ is the nodal value at time t_l , $l = 1, \dots, m$, of the i^{th} component of u at the j^{th} node in the spatial FEM mesh, is reshaped into

$$y = (y_1 \ y_2 \ \dots \ y_m) = \begin{pmatrix} u_{1,1}(0) & u_{1,1}(t_1) & \dots & u_{1,1}(1) \\ u_{1,2}(0) & u_{1,2}(t_1) & \dots & u_{1,2}(1) \\ \vdots & \vdots & \dots & \vdots \\ u_{1,n_p}(0) & u_{1,n_p}(t_1) & \dots & u_{1,n_p}(1) \\ u_{2,1}(0) & u_{2,1}(t_1) & \dots & u_{2,1}(1) \\ \vdots & \vdots & \dots & \vdots \\ u_{N,n_p}(0) & u_{N,n_p}(t_1) & \dots & u_{N,n_p}(1) \end{pmatrix}. \quad (49)$$

Note that in this setting we have a certain redundancy $y_1 = y_m$ from the periodic in time boundary conditions, which however turns out to be convenient for the implementation. TOM requires separated boundary conditions, and thus we pad y and the temporal discretization $t = (0, t_2, \dots, t_{m-1}, 1)$ in the form (TOM needs a multiple of 5 temporal discretization points, even though we only use a second order (in time) method)

$$\begin{aligned} \tilde{t} &= (-(1-t_{m-2}), -(1-t_{m-1}), 0, t_2, \dots, t_{m-1}, 1, 1+t_2, 1+t_3, 1+t_4), \\ \tilde{y} &= (y_{m-2}, y_{m-1}, y_1, y_2, \dots, y_{m-1}, y_m, y_2, y_3, y_4). \end{aligned}$$

Then we obtain \mathcal{G} and $\partial_u \mathcal{G}$ from adding some dummy BC at $-(1-t_{m-2})$ and $1+t_m$, plugging this into TOM, and extracting components 3 to $m+2$ from the resulting $\tilde{\mathcal{G}}$ and re-sorting the Jacobian

$\partial_{\tilde{y}}\mathcal{G}$. $\partial_u\mathcal{G}$ then has the form, as TOM uses backward differences for \dot{u} ,

$$\begin{pmatrix} \bullet & 0 & 0 & 0 & \dots & \bullet & 0 \\ \bullet & \bullet & 0 & 0 & \dots & 0 & 0 \\ 0 & \bullet & \bullet & 0 & \dots & 0 & 0 \\ \vdots & \dots & \ddots & \ddots & \ddots & 0 & 0 \\ 0 & \dots & \dots & \ddots & \ddots & 0 & 0 \\ 0 & \dots & \dots & 0 & \bullet & \bullet & 0 \\ 0 & \dots & \dots & \dots & 0 & \bullet & \bullet \end{pmatrix}. \quad (50)$$

Here, each $0 \in \mathbb{R}^{n_u \times n_u}$, and \bullet stands for a (sparse) $n_u \times n_u$ matrix, which is assembled from $M\dot{u}(t_l)$ and the standard `pde2path` routines for $\partial_u G$. The derivatives $\partial_T\mathcal{G}, \partial_\lambda\mathcal{G}$ are cheap from numerical differentiation, and $\partial_u\phi$ and τ do not change during Newton loops, and are easily taken care of anyway.

B hopflib library overview

Our Hopf setup does not need any user setup additional to the functions such as `p.fuha.sG`, `p.fuha.sGjac` (or `p.fuha.G`, `p.fuha.Gjac`) already needed to describe stationary problems. Moreover, the only changes of the core `p2plib` concern some queries whether we consider a Hopf problem, in which case the basic routines such as `cont` call a Hopf version, i.e., `hocont`. HBPs are flagged by `p.sol.ptype=3`, while points on a Hopf branch have `p.sol.ptype=4`. The natural parametrization (§2.3.3) for periodic orbit continuation is flagged by `p.sw.param=3`, while `p.sw.param=4` flags `arclength` (§2.3.2).

The `hopflib` related variables are collected in the field `p.hopf`, see Table 4, while Table 5 summarizes the main functions from `hopflib`. See also [DRUW14, App.A] for the general organization of `p.fuha` (function handles), `p.nc` (numerical controls), `p.sw` (switches), `p.plot` (plot settings), `p.file` (file handling), `p.sol` (solution at runtime), etc in `p`.

Table 4: Entries in `p.hopf` (first block), and additions/modifications to `p.nc`.

field	purpose
y	for <code>p.sw.param=4</code> : unknowns in the form (49) ($n_u \times m$ matrix);
y0d	for <code>p.sw.param=3</code> : augmented by \tilde{y} and T, λ ($(2n_u+2) \times m$ matrix).
tau	for <code>p.sw.param=4</code> : $M\dot{u}_0$ for the phase condition (18) ($n_u \times m$ matrix);
ysec	for <code>p.sw.param=3</code> : $M\dot{u}_0(0)$ for the phase condition (32) ($2n_u+2$ vector).
t,tl	tangent, see (23)
lam, T	secant between two solns $(y_0, T_0, \lambda_0), (y_1, T_1, \lambda_1)$ for <code>p.sw.param=3</code> ; $(2n_u+2) \times m$ matrix
xi,wT	time discretization vector, and its length
x0i	current param.value and period
plot	weights for the arclength, see (20)
wn	index for plotting $t \mapsto u(\vec{x}(x0i))$
tom	aux. vars to control hoplot during hocont; see the description of <code>hoplot</code> ; default <code>plot=[]</code>
jac	struct containing the winding number related settings for <code>initedig</code>
p.nc.mu1	struct containing TOM settings, including the mass matrix M
p.nc.mu2	switch to control assembly of $\partial_u\mathcal{G}$. <code>jac=0</code> : numerically (only recommended for testing);
p.nc.eigref	<code>jac=1</code> : via <code>hosjac</code> , which uses <code>p.fuha.Gjac</code> . Note that for <code>p.sw.jac=1</code> the local matrices $\partial_u G(u(t_j))$ are still assembled via <code>p.fuha.sGjac</code> .
	for <code>bifcheck=2</code> : start bisection if <code>ineg</code> changed, and $ \operatorname{Re}(mu) < \mu1$; assume $\operatorname{Re}(\mu) = 0$ (BP or HP) if $ \operatorname{Re}(\mu) < \mu2$ at end of bisection
	now a vector (in general), as is <code>p.nc.neig</code>

Table 5: Overview of main functions related to Hopf bifurcations

name	purpose
hoswibra	see (16), and comments below
hobra	standard-setting for p.fuha.outfu (data on branch), but might be necessary to adapt to a given problem
hostanufu	standard setting for screen printout, see also hostanheadfu
hoplot	plot the data contained in hopf.y. Space-time plot in 1D; in 2D and 3D: snapshots at (roughly) $t = 0$, $t = T/4$, $t = T/2$ and $t = 3T/4$; see also hoplotf;
initeig	find guess for ω_1 ; see also initwn
hotintxs	time integrate (3) from the data contained in p.hopf and u0, with output of $\ u(t) - u_0\ _\infty$, and saving $u(t)$ to disk at specified values
tintplot*d	plot output of hotintxs; $x-t$ -plots for $*$ =1, else snapshots at specified times
initwn	init vectors for computation of g from (11)
hogetnf	compute initial guess dlam, al for the coefficients of bifurcating Hopf branch from the normal form (12)
hocont	main continuation routine; called by cont if p.sol.ptype>2
hostanopt, hoMini	standard options for, and initialization of hopf.tom
hoinistep	perform 2 initial steps and compute secant, used if p.sw.param=3
honloopext, honloop	the arclength Newton loop (26), and the Newton loop with fixed λ
tomsol	use TOM to solve (33)
tomassemG, tomassem	use TOM to assemble \mathcal{G} , or $(\mathcal{G}, \partial_u \mathcal{G}, \partial_T \mathcal{G}, \partial_\lambda \mathcal{G})$, respectively
tomassemphc	pad y and assemble with periodic BC; calls tomassemG and tomassem
gethoA	put together the extended Jacobian \mathcal{A} from (26)
hopc	the phase condition ϕ from (18) and $\partial_u \phi$ from (22)
arc2tom, tom2arc	convert arclength data (49) to tomsol data $(y; \tilde{y}; T; \lambda)$, e.g., to call tomsol for meshadaption. tom2arc to go back.
ulamcheckho	check for and compute solutions at user specied values in p.usrlam
hosrhs, hosrhsjac	interfaces to p.fuha.G and p.fuha.Gjac at fixed t , internal functions called by tomassemphc, together with hodummybc
horhs, hojac, hobb(jac)	similar to hosrhs, horhsjac, for (33)

As Table 5 is only intended as an overview, we refer to the source code, and the demo directories, for the exact arguments and further details on the `hopflib` functions. Besides `cont`, the functions `initeig`, `hoswibra`, `hoplot`, `hotintxs`, and `tintplot*d` are most likely to be called directly by the user, and `hobra` and `hostanufu` are likely to be adapted by the user. The functions involving TOM, and those with rhs or jac in their name are basically described in §2. As usual, all functions in Table 5 can be most easily overloaded by copying them to the given problem directory and modifying them there, but the three demos from §4 run with the standard functions as contained in `hopflib`.

In `p=hoswibra(dir,fname,ds,para,varargin)`, the auxiliary argument `aux=varargin{2}` (`varargin{1}` is the new directory) can for instance have the following fields:

- `aux.tl=20`: (initial, i.e., might be refined for `p.sw.param=3`) number of (equally spaced) mesh-points in $t \in [0, 1]$. For larger scale problems, i.e., with more than 2000 DoF in space, we recommend to at least initially reduce `tl` to 10, see, e.g., `cGL/cGL2dcmds.m`, `cGL/cGL3dcmds.m`, `rot/rotcmds.m` and `bru/bru2dcmds.m`.
- `aux.al`, `aux.dlam` (no preset): can be used to pass a guess for α and $s=dlam$ from (12) and thus circumvent `hogetnf`; useful for quasilinear problems, see footnote 4.

`hoplot(p,wnr,cnr,varargin)`, where `wnr` and `cnr` are the window number and component number, is the basic plotting routine for periodic orbits, contained in `p.hopf.y`. The auxiliary argument `aux=varargin` can contain a number of fields used to control its behaviour. Examples are (with default values as indicated)

- `aux.lay=[2 2]`: sets the subplot-layout for the snapshots (in 2D)

- `aux.pind=[]`; set the indices, i.e., the times `T*p.hopf.t(aux.pind)`, to be used for plotting; if `pind=[]`, then the four indices 1, `tl/4`, `tl/2`, `3*tl/4` are used.
- `aux.xtics=[]`; set `xtics`, similar for `ytics` and `ztics`; see also `aux.cb`. (colorbar on/off)

This provides some flexibility for plotting time snapshots of periodic orbits in 2D and 3D. However, most likely the user will adapt `hoplot` to the problem; see, e.g., the examples `hoplotrot` and `hoplotbru` in the demo directories `rot` and `bru`.

C Some implementation details

We exemplarily comment on how to set up and run (35), i.e.,

$$\partial_t \begin{pmatrix} u_1 \\ u_2 \end{pmatrix} = \begin{pmatrix} \Delta + r & -\nu \\ \nu & \Delta + r \end{pmatrix} \begin{pmatrix} u_1 \\ u_2 \end{pmatrix} - (u_1^2 + u_2^2) \begin{pmatrix} c_3 u_1 - \mu u_2 \\ \mu u_1 + c_3 u_2 \end{pmatrix} - c_5 (u_1^2 + u_2^2) \begin{pmatrix} u_1 \\ u_2 \end{pmatrix} \quad (51)$$

over 1D, 2D and 3D rectangles with homogeneous Neumann or Dirichlet BC in `pde2path`. In 1D, the initialization is (l3-6 of `cGL1dcmds.m`)

```
ndim=1; dir='hom1d'; p=[]; lx=pi; nx=30;
par=[-0.05; 1; 0.1; -1; 1]; % r nu mu c3 c5
p=cGLinit(p,lx,nx,par,ndim);
```

where we use the domain size `lx`, the number `nx` of points in the spatial discretization, the base parameter set `par` from (36), and the space dimensions `ndim` as parameters. However, `ndim` only plays a role in l5–l14 of the `init` routine:

```
function p=cGLinit(p,lx,nx,par,ndim)
p=stanparam(p); screenlayout(p); % set standard parameters and screenlayout
p.nc.neq=2; p.nc.ilam=1; p.fuha.outfu=@hobra; % number of eq, cont-param, output
p.fuha.Gjac=@Gjac; p.fuha.sG=@sG; p.fuha.sGjac=@sGjac; p.sw.jac=1; % rhs and Jac
5 switch ndim % set domain and BC depending on ndim
    case 1; pde=stanpdeo1D(lx,2*lx/nx); p.vol=2*lx; p.hopf.x0i=1;
        bc=pde.grid.neumannBC('0'); % OOPDE BC syntax
    case 2; pde=stanpdeo2D(lx,lx/2,2*lx/nx); p.vol=2*lx^2; p.hopf.x0i=30;
        bc=pde.grid.dirichletBC('1','0');
10 case 3; pde=stanpdeo3D(lx,lx/2,lx/4,2*lx/nx); p.vol=0.5*lx^3; p.hopf.x0i=200;
        bc=pde.grid.dirichletBC('1','0');
        p.plot.ng=20; % settings for 3D plots (somewhat problem dependent)
        p.plot.levc={'blue','red'}; p.plot.lev=[-0.1 0.1]; p.plot.alpha=0.5;
end
15 pde.grid.makeBoundaryMatrix(bc); p.nc.sf=1e3; % OOPDE set up of BC for assemb
p.pdeo=pde; p.sw.sfem=-1; p.np=pde.grid.nPoints; p.nu=p.np*p.nc.neq;
p.sol.xi=1/p.nu; p=setfemops(p); % setfemops calls oosetfemops in problem dir
u=0*ones(p.np,1); v=u; p.u=[u;v]; p.u(p.nu+1:p.nu+5)=par; % initial guess
p.usrlam=[-0.25 -0.2 -0.1 0 0.5 1 2 3]; % user-vals for lambda (output)
20 p.file.smod=10; p.plot.cm=hot; p.plot.bpcmp=9; % saving, colormap, and branch-plot
```

In 1D the choice of `x0i` is somewhat arbitrary due to the Neumann BC, but in 2D and 3D $x(x0i)$ should not be on the boundary due to the Dirichlet BC. To set up the BC we use the OOPDE routines `pde.grid.neumannBC` and `pde.grid.dirichletBC` in l7, l9 and l11, respectively, such that the call of `pde.grid.makeBoundaryMatrix` in l15 can take care of the rest, where the Dirichlet BC are implemented via a stiff spring approximation; see [Prü16] for details.

The crucial files to implement (51) and the BC are thus `oosetfemops.m`, `sG.m` and `sGjac.m`, which read

```
1 function p=oosetfemops(p) % in problem-dir since highly problem dependent
2 [K,M,~]=p.pdeo.fem.assemb(p.pdeo.grid,1,1,1); % stiffness/mass matrix (1 comp)
3 [Q,G,H,R]=p.pdeo.fem.assemb(p.pdeo.grid); % matrices for BC (empty for Neumann BC)
4 % augment K and M to 2-compos, and add BC matrices to K
```

```

5 sf=p.nc.sf; N=sparse(p.np, p.np); % stiffness factor, and dummy N
6 p.mat.K=[K+sf*(H'*H) N]; [N K+sf*(H'*H)]; p.mat.M=[M N]; [N M];
7 end

```

```

1 function r=sG(p,u) % compute pde-part of residual
2 f=honf(p,u); r=p.mat.K*u(1:p.nu)-p.mat.M*f;

```

```

1 function Gu=sGjac(p,u) % compute pde-part of Jacobian
2 [f1u,f1v,f2u,f2v]=njac(p,u); n=p.np;
3 Fu=[spdiags(f1u,0,n,n),spdiags(f1v,0,n,n)];
4 [spdiags(f2u,0,n,n),spdiags(f2v,0,n,n)];
5 Gu=p.mat.K-p.mat.M*Fu;
6 end

```

In `oosetfemops.m` we first assemble the one component Neumann Laplacian stiffness matrix K , the 1-component mass matrix M , and then the 1-component BC matrices Q, H , which implement the boundary conditions previously set in `cGLinit.m`, l7, 9, 13, respectively. Then in l7 we put together the true system matrices “by hand”. So far we find this most convenient, but refer to [Prü16] for more sophisticated ways to set up systems and more complicated BC directly. Also note that here for the Dirichlet BC in 2D and 3D we use the typical stiff spring approximation with stiffness factor `sf`, and the matrix Q and the vectors G, R (again see [Prü16]) are not used.

The function `sG.m` uses the stiffness and mass matrices K and M , and calls `nodalf.m` to compute the nonlinear terms, and is otherwise completely generic; `nodalf.m`, which is also called in `hogetnf.m` for the computation of the normal form coefficients reads

```

1 function f=nodalf(p,u) % the 'nonlinearity' (i.e., everything except diffusion)
2 % for cGL, directly defined via the nodal values of u1=Re(u) and u2=Im(u)
3 u1=u(1:p.np); u2=u(p.np+1:2*p.np); us=u1.^2+u2.^2; par=u(p.nu+1:end);
4 r=par(1); nu=par(2); mu=par(3); c3=par(4); c5=par(5);
5 f1=r*u1-nu*u2-us.*(c3*u1-mu*u2)-c5*us.^2.*u1;
6 f2=r*u2+nu*u1-us.*(c3*u2+mu*u1)-c5*us.^2.*u2;
7 f=[f1;f2];
8 end

```

After the extraction in l3 of the two components u_1 and u_2 and of the parameters from the internal solution vector u , the rhs from (51) is simply typed in. Similarly, `njac` from `sGjac.m`, l2, is the derivative of f , and thus easily typed in as well (see `njac.m`). All these files, i.e., `oosetfemops.m`, `sG.m`, `sGjac.m` and the nonlinearity `nodalf.m`, are completely dimension independent.

After the initialization `p=cGLinit(.)`, in `cGL1dcmds` we (re)set the output directory, the continuation step-length, and, most importantly, `bifcheck=2`, and then simply call `cont`:

```
p=setfn(p,dir); p.sol.ds=0.1; p.sw.bifcheck=2; p.nc.neig=10; p=cont(p,20);
```

This finds a number of (Hopf) bifurcation points from the trivial branch $u \equiv 0$. Then we call `hoswibra` (here for the first HP) and `cont` again:

```

1 para=4; ds=0.1; p=hoswibra('hom1d','hpt1',ds,para,'1dbl'); % p.sw.verb=2;
2 p.fuha.blss=@mbel; p.nc.mbw=2; % p.hopf.ilss=1; % set to 0 if no ilupack
3 p=cont(p,10);

```

Uncommenting `p.sw.verb=2` (verbosity switch) in l1 gives more output, and `p.hopf.ilss=1` in l2 turns on the `ilupack` iterative solver in `mbel`.

Except for an exemplarily call of `hoswibra` with `para=3`, the remainder of the script file `cGL1dcmds.m` consists of plotting and stability check commands, and we refer to the script for comments. The 2D and 3D scripts `cGL2dcmds.m` and `cGL3dcmds.m` follow the same rules, and similarly do the scripts for the `rot` and `bru` demos. The main difference of the `rot` demo to the other two is that in `rot` we do not use OOPDE, such that the BC are set via `gnbc.m`, the system matrices are set directly via `setfemops.m` in a more convenient way, and there is no `oosetfemops.m` file. As already said, each demo directory contains some auxiliary functions or scripts, for instance

cGL/plotana.m used for plotting the analytical comparisons in Figs. 3 and 4, or rot/auxcmds.m which contains commands to create a movie of the rotating patterns, or bru/auxcmds.m which gives examples of how adaptive spatial mesh refinement can be used, cf. Remark 4.2.

References

- [Bol11] M. Bollhöfer. ILUPACK V2.4, <http://www.icm.tu-bs.de/bolle/ilupack/>, 2011.
- [DGK03] E. J. Doedel, W. Govaerts, and Yu. A. Kuznetsov. Computation of periodic solution bifurcations in ODEs using bordered systems. *SIAM J. Numer. Anal.*, 41(2):401–435, 2003.
- [Doe07] E. J. Doedel. Lecture notes on numerical analysis of nonlinear equations. In *Numerical continuation methods for dynamical systems*, pages 1–49. Springer, Dordrecht, 2007.
- [DRUW14] T. Dohnal, J. Rademacher, H. Uecker, and D. Wetzel. pde2path 2.0. In H. Ecker, A. Steindl, and S. Jakubek, editors, *ENOC 2014 - Proceedings of 8th European Nonlinear Dynamics Conference*, ISBN: 978-3-200-03433-4, 2014.
- [DU16] T. Dohnal and H. Uecker. Bifurcation of Nonlinear Bloch waves from the spectrum in the nonlinear Gross-Pitaevskii equation. To appear in *J. Nonlinear Sci.*, 2016.
- [GKS00] M. Golubitsky, E. Knobloch, and I. Stewart. Target patterns and spirals in planar reaction-diffusion systems. *J. Nonlinear Sci.*, 10(3):333–354, 2000.
- [Gov00] W. Govaerts. *Numerical methods for bifurcations of dynamical equilibria*. SIAM, 2000.
- [GS96] W. Govaerts and A. Spence. Detection of Hopf points by counting sectors in the complex plane. *Numer. Math.*, 75(1):43–58, 1996.
- [GS02] M. Golubitsky and I. Stewart. *The symmetry perspective*. Birkhäuser Verlag, Basel, 2002.
- [HBK⁺96] N. Hartmann, M. Bär, I. G. Kevrekidis, K. Krischer, and R. Imbihl. Rotating chemical waves in small circular domains. *PRL*, 76(8), 1996.
- [Kue15a] Chr. Kuehn. Efficient gluing of numerical continuation and a multiple solution method for elliptic PDEs. *Appl. Math. Comput.*, 266:656–674, 2015.
- [Kue15b] Chr. Kuehn. Numerical continuation and SPDE stability for the 2D cubic-quintic Allen-Cahn equation. *SIAM/ASA J. Uncertain. Quantif.*, 3(1):762–789, 2015.
- [Kuz04] Yu. A. Kuznetsov. *Elements of applied bifurcation theory*, volume 112 of *Applied Mathematical Sciences*. Springer-Verlag, New York, third edition, 2004.
- [Mei00] Z. Mei. *Numerical bifurcation analysis for reaction-diffusion equations*, volume 28 of *Springer Series in Computational Mathematics*. Springer-Verlag, Berlin, 2000.
- [MT04] F. Mazzia and D. Trigiante. A hybrid mesh selection strategy based on conditioning for boundary value ODE problems. *Numerical Algorithms*, 36(2):169–187, 2004.
- [Prü16] U. Prüfert. OOPDE: FEM for Matlab, www.mathe.tu-freiberg.de/nmo/mitarbeiter/uwe-pruefert/software, 2016.
- [SDE⁺15] E. Siero, A. Doelman, M. B. Eppinga, J. D. M. Rademacher, M. Rietkerk, and K. Siteur. Striped pattern selection by advective reaction-diffusion systems: resilience of banded vegetation on slopes. *Chaos*, 25(3), 2015.
- [Sey10] R. Seydel. *Practical bifurcation and stability analysis. 3rd ed.* Springer, 2010.
- [Uec15] H. Uecker. The pde2path add-on library p2poc for solving o infinite timehorizon spatially distributed optimal control problems - Quickstart Guide. Preprint, 2015.
- [Uec16a] H. Uecker. Optimal harvesting and spatial patterns in a semi arid vegetation system. To appear in *Natural Resource Modelling*, 2016.
- [Uec16b] H. Uecker. pde2path, www.staff.uni-oldenburg.de/hannes.uecker/pde2path, 2016.

- [UW14] H. Uecker and D. Wetzel. Numerical results for snaking of patterns over patterns in some 2D Selkov-Schnakenberg Reaction-Diffusion systems. *SIADS*, 13-1:94–128, 2014.
- [UWR14] H. Uecker, D. Wetzel, and J. Rademacher. pde2path – a Matlab package for continuation and bifurcation in 2D elliptic systems. *NMTMA*, 7:58–106, 2014.
- [Wet16] D. Wetzel. Pattern analysis in a benthic bacteria-nutrient system. *Math. Biosci. Eng.*, 13(2):303–332, 2016.
- [YDZE02] L. Yang, M. Dolnik, A. M. Zhabotinsky, and I. R. Epstein. Pattern formation arising from interactions between Turing and wave instabilities. *J. Chem. Phys.*, 117(15):7259–7265, 2002.
- [YE03] L. Yang and I. R. Epstein. Oscillatory Turing patterns in reaction–diffusion systems with two coupled layers. *PRL*, 90(17):178303–1–4, 2003.
- [ZHKR15] D. Zhelyazov, D. Han-Kwan, and J. D. M. Rademacher. Global stability and local bifurcations in a two-fluid model for tokamak plasma. *SIAM J. Appl. Dyn. Syst.*, 14(2):730–763, 2015.